U.PORTO
FACULDADE DE CIÊNCIAS
UNIVERSIDADE DO PORTO

MSc

2.º CICLO

FCUP
ICBAS
CNPP
2016

U.PORTO

Brainstem plasticity following long-term adaptation of the vestibulo-ocular reflex

Filipa França de Barros

FC

U.PORTO
FACULDADE DE CIÊNCIAS
UNIVERSIDADE DO PORTO

U.PORTO
INSTITUTO DE CIÊNCIAS BIOMÉDICAS ABEL SALAZAR
UNIVERSIDADE DO PORTO

Centre de Neurophysique, Physiologie et Pathologie
UMR 8119

UNIVERSITÉ PARIS DESCARTES

Brainstem plasticity following long-term adaptation of the vestibulo-ocular reflex

Filipa França de Barros

Master's Dissertation presented to Faculty of Sciences of the University of Porto, Institute of Biomedical Sciences Abel Salazar of the University of Porto

Biochemistry

2016

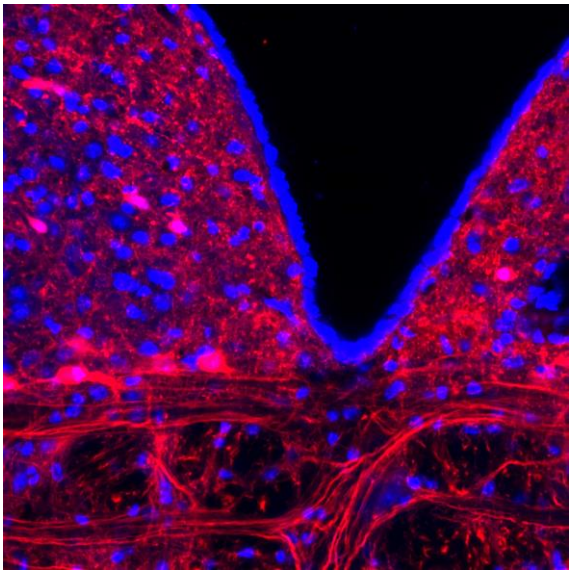

Brainstem plasticity following long-term adaptation of the vestibulo-ocular reflex

Filipa França de Barros

Master in Biochemistry
Department of Chemistry and Biochemistry
2016

Supervisors
Dr. Mathieu Beraneck, team leader, *Centre de Neurophysique,Physiologie et Pathologie,* Paris

Dr. Julie Carcaud, pos-doctoral fellow, *Centre de Neurophysique,Physiologie et Pathologie,* Paris

Centre de Neurophysique, Physiologie et Pathologie UMR 8119

UNIVERSITÉ PARIS DESCARTES

U.PORTO

INSTITUTO DE CIÊNCIAS BIOMÉDICAS ABEL SALAZAR
UNIVERSIDADE DO PORTO

U.PORTO

FACULDADE DE CIÊNCIAS
UNIVERSIDADE DO PORTO

Todas as correções determinadas pelo júri, e só essas, foram efetuadas.

O Presidente do Júri,

Porto, _____/_____/_____

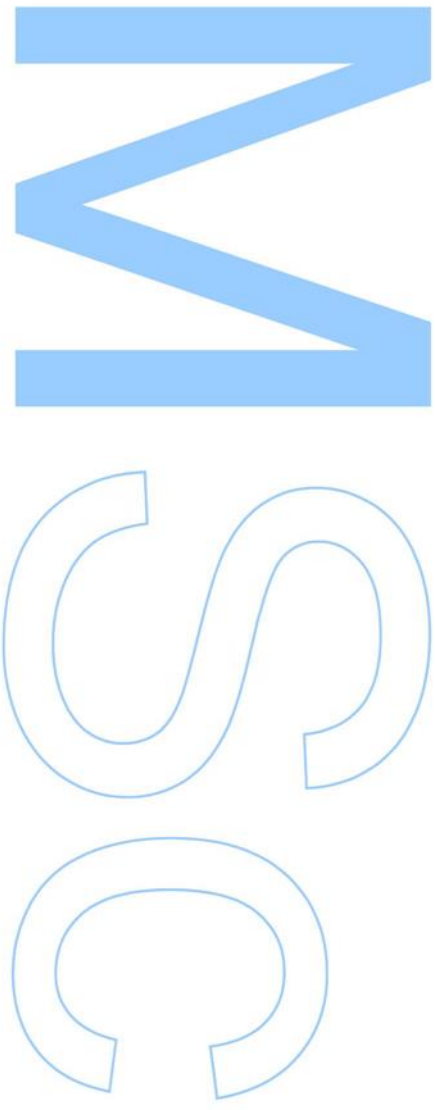

Acknowledgements

I am extremely grateful to Mathieu. Thank you for the support, advices and orientation that you provided me from the very beginning. Above all, thank you for accepting me and making me a part of this wonderful team. Thank you for teaching me the true meaning of *serendipity*.

To Julie, an enormous thank you. I could not have had a better scientist by my side. Thank you for sharing with me all the techniques and skills as well as the professional values and work ethics which have greatly shaped me. Thank you for all the time, effort and dedication spent through the year and especially thank you for letting me know you.

I am especially thankful for having encountered Mélanie, my colleague and good friend with whom I shared every moment in the lab's office. Thank you for hearing me sing out of key so many times! To Michele a thank you for, since the first day, being so welcoming and also for sharing interesting stories.

Thank you to David, Desdemona and Mérie for providing the team with great partnership and innovative spirit. A big thank you to everyone at the CNPP including its director, Claude Meunier, to whom I am grateful for all the support and daily kindness.

Agradeço ao Professor Pedro Fernandes pelo seu espírito alegre e positivo que me contagiou durante todo o Mestrado.

Muito obrigada Mami, Papi e Raquel por sempre acreditarem em mim e me apoiarem diariamente. Obrigada também pelas vossas visitas a Paris que me ajudaram a matar um bocado das saudades que senti.

Por todos estes anos da tua fiel companhia, muito obrigada Foxy. Este trabalho também é dedicado a ti.

Muito obrigada André, meu companheiro nesta grande viagem que é a vida.

Abstract

The ability to orientate in space is crucial for survival. This behavior relies on the neural representation that emerges from the integration of various sensory inputs. Through the detection of gravity, the vestibular system plays a central role in self-motion perception. Since it detects the motion of the head in space, it unravels fundamental sensorimotor functions such as balance, posture or gaze stabilization. These functions are kept constant through life as a result of the adaptation to the surrounding visual and vestibular inputs. By performing a visuo-vestibular mismatch (VVM) protocol, we demonstrate that the long-term exposure to a conflict between these inputs causes a lasting adaptation of the vestibulo-ocular reflex (VOR). This adaptive motor memory, which initially is generated and stored in the cerebellum, is on the long term transferred to the vestibular nuclei. Hence, using a video-oculography technique in mice that underwent the VOR adaptation protocol, we were able to determine that the adaptation persists for several days, it is frequency-dependent and that a strong retinal slip drives motor learning. Additionally, to investigate the cellular and molecular mechanisms underlying this long-term adaptation we performed whole-cell patch clamp in brainstem slices in both control mice and mice adapted to the VVM. The central vestibular neuron's synaptic activity was recorded while the vestibular afferents were stimulated with a bipolar electrode. The gathered electrophysiological results suggest that, the efficacy of the synapse that connects the vestibular afferents to the vestibular nuclei is compromised following long-term adaptation. Using immunohistochemistry, we tested a possible basis of the observed modifications in the vestibular nuclei neurons' synaptic properties. Additionally, using mice displaying fluorescent GABAergic neurons, we performed encouraging preliminary studies that, further on, will allow determining the role of the different subpopulation of neurons in the adaptive process. In conclusion, the present study shows that consolidation of long-term VOR adaptation relies on synaptic plasticity in the direct VOR pathway.

Key-words: VOR, adaptation, motor learning, vestibular, brainstem.

Resumo

A capacidade de orientação no espaço é crucial para a sobrevivência. Este comportamento depende da representação neural que emerge da integração de vários *inputs* sensoriais. Através da deteção da gravidade, o sistema vestibular exerce um papel central na perceção do deslocamento individual no espaço. Pela deteção do movimento da cabeça no espaço, possibilita funções sensoriomotoras fundamentais como o equilíbrio, a postura ou a estabilização do olhar. Estas funções são mantidas constantes ao longo da vida como resultado da adaptação aos *inputs* visuais e vestibulares circundantes. Realizando um protocolo de desemparelhamento visuo-vestibular (VVM), neste estudo demostrou-se que a exposição a longo prazo ao conflito entre estes dois inputs causa uma adaptação duradoura do reflexo vestíbulo-ocular (VOR). Esta memória motora adaptativa, que inicialmente é gerada e guardada no cerebelo, é a longo prazo transferida para o núcleo vestibular. Assim, usando a técnica de vídeo-oculografia em ratinhos que foram sujeitos ao protocolo de adaptação do VOR, neste estudo determinamos que a adaptação persiste durante vários dias, é dependente da frequência e que o deslizamento da imagem na retina conduz a aprendizagem motora. De modo a investigar os mecanismos moleculares e celulares adjacentes a esta adaptação de longo-termo, realizou-se *whole-cell patch clamp* em cortes de tronco cerebral de ratinhos controlo e ratinhos submetidos ao protocolo de VVM. A atividade sináptica dos neurónios centrais vestibulares foi gravada enquanto o aferente vestibular foi estimulado com um elétrodo bipolar. Os resultados eletrofisiológicos reunidos sugerem que a eficácia da sinapse que liga o aferente vestibular ao núcleo vestibular, fica comprometida após a adaptação de longo prazo. Usando imunohistoquímica foi também testada uma possível base das modificações observadas nas propriedades sinápticas dos neurónios do núcleo vestibular. Adicionalmente, usando ratinhos com neurónios GABAérgicos fluorescentes, realizamos estudos preliminares que, no futuro, permitirão determinar o papel das diferentes subpopulações de neurónios no processo adaptativo. Em conclusão, o presente estudo mostra que a consolidação de longo-termo da adaptação do VOR requer plasticidade sináptica na via direta do reflexo vestíbulo-ocular.

Palavras-chave: VOR, adaptação, aprendizagem motora, vestibular, tronco cerebral.

Table of contents

List of Figures and Tables

List of Abbreviations

ACSF	artificial cerebrospinal fluid
AHP	after-hyperpolarization
AHPR	after-hyperpolarization rectification
AMPA	α-amino-3-hydroxy-5-methyl-4-isoxazolepropionic acid
ANOVA	analysis of Variance
AUC	area under the curve
BBS	borate buffered saline
CC	current clamp
CF	climbing fibers
dAHP	double after-hyperpolarization
DAPI	4',6-diamidino-2-phenylindole
DVN	descending vestibular nuclei
eEPSC	evoked excitatory post-synaptic current
EOM	extraocular muscles
FTN	flocculus target neurons
GAD67	glutamic acid decarboxylase 67
GIN	GFP-expressing inhibitory neurons
HVOR	horizontal vestibulo ocular reflex
IF	current-frequency
IV	current-voltage
LVN	lateral vestibular nucleus
MVN	medial vestibular nucleus
NGS	normal goat serum

NMDAr	N-methyl-D-aspartate receptor
OKR	optokinetic reflex
PBS	phosphate-buffered saline
PFA	Paraformaldehyde
Pvalb-Cre	parvalbumine-cre
PVP	position-vestibular-pause neurons
RT	room temperature
Sst-Cre	somatostatine-cre
SVN	superior vestibular nucleus
VC	voltage clamp
VN	vestibular nucleus
VOR	vestibulo-ocular reflex
VVM	visuo-vestibular mismatch
YFP	yellow fluorescent protein
1º VNs	first-order vestibular neurons
2ºVNs	second-order vestibular neurons

Introduction

1. The vestibular system

1.1. Function of the Vestibular system

In the *De Anima* book II, Aristoteles described for the first time the five senses: sight, hearing, taste, smell and touch (Durrant and Aristotle, 1993, Cullen, 2012). These sensory systems were indubitably appreciated since antiquity because they provide us with recognizable and distinct everyday life perceptions. Remarkably, the vestibular system was one of the earliest sensory systems to rise in evolution and it is phylogenetically the oldest part of the inner ear (Cullen, 2012). Conversely, after many close attempts (**Figure 1**), it was the last one to be discovered and was only considered an entity distinct from the cochlea in the middle of the 19th century by Pierre-Marie Flourens, a French physiologist (Wiest, 2015).

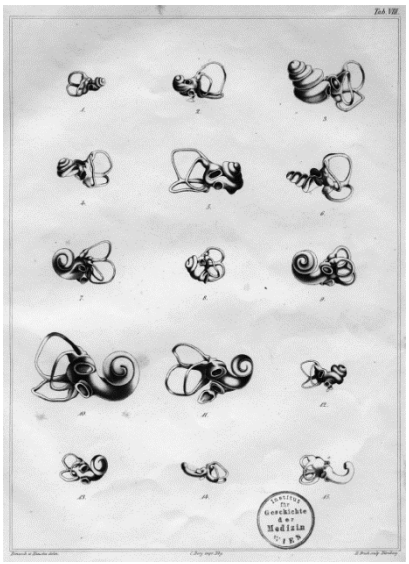

Figure 1. Image of Josef Hyrtl's collection of inner ears of different species from his published textbook in 1845. Based on their shape, Hyrtl erroneously assumed that the semicircular canals served the function of condensing sound waves. From (Wiest, 2015).

The vestibular system participates in a wide range of functions, from reflexes to the most intricate level of voluntary behavior and bears information about head motion and position relative to gravity. Although it has a key role in daily life, this late recognition was mainly due to the fact that, when this system is functioning correctly, we are unaware of the information coming from vestibular activity, so that there is no vestibular perception in normal situation. Normally, vestibular, visual and proprioceptive inputs are seamlessly

integrated to give rise to internal estimates of motion as well as the coordination of oculomotor and postural movements. Obtrusive vestibular sensations appear when there is an abnormal motion or pathology that involves the peripheral organs or their central pathways. These sensations are commonly known as vertigo, dizziness or imbalance (Kandel, 2013).

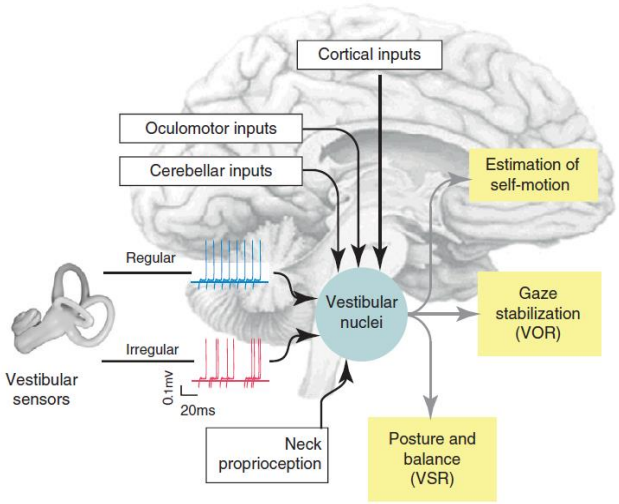

Figure 2. Multimodal integration within vestibular pathways. The brain areas vestibular nuclei (VN) receive direct inputs and the outputs of the processing of the information. From (Cullen, 2012)

In order to maintain proper locomotion and to stabilize gaze and posture, the vestibular system encodes the self-motion information through the detection of the motion of the head in space (Beraneck and Idoux, 2012). Combining oculomotor, cerebellar, cortical inputs as well as neck proprioception and inputs from the vestibular sensors, the vestibular nuclei will generate the estimation of self-motion, and premotor command for gaze stabilization reflexes, as well as posture and balance reflexes (**Figure 2**).

1.2. Anatomy and Physiology

The vestibular system is a distributed system that gathers the peripheral vestibular apparatus, the brainstem central vestibular nuclei, parts of the cerebellum (nodulus, uvula, flocculus & paraflocculus), and various areas of the cerebral cortex (Khan and Chang 2013).

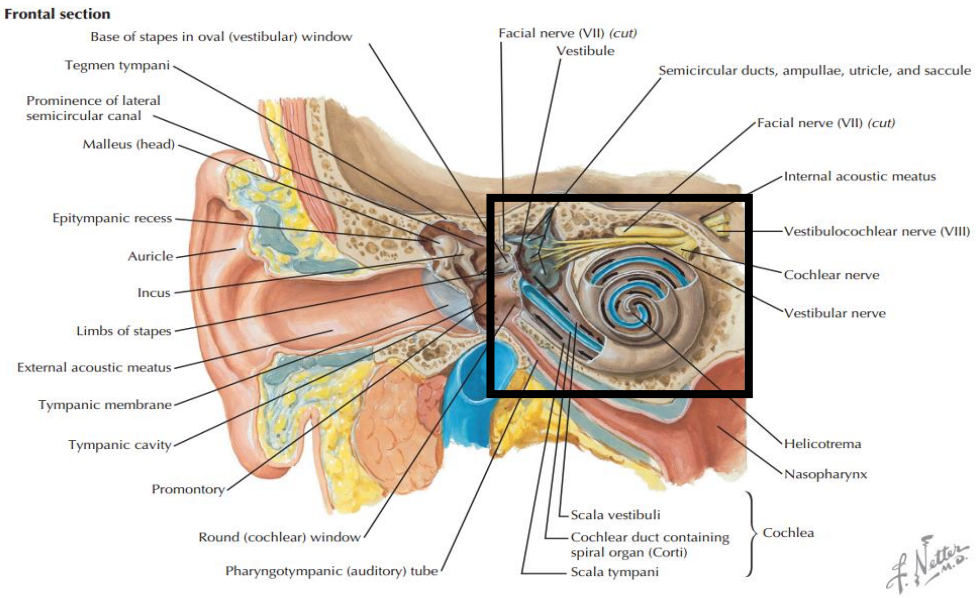

Figure 3. Anatomy of the ear. Black square indicates the inner ear. From (Felten et al., 2003).

The inner ear possesses five peripheral vestibular structures: the utricle, the saccule and the three semicircular canals (anterior, posterior and horizontal) (**Figure 3**). These small structures constitute the vestibular apparatus and detect head motion and gravitational force (Highstein and McCrea, 1988)

1.2.1. Bony and membranous labyrinth

The peripheral vestibular apparatus is located in the inner ear, more specifically, on the temporal bone, and it comprises the bony labyrinth and membranous labyrinth.

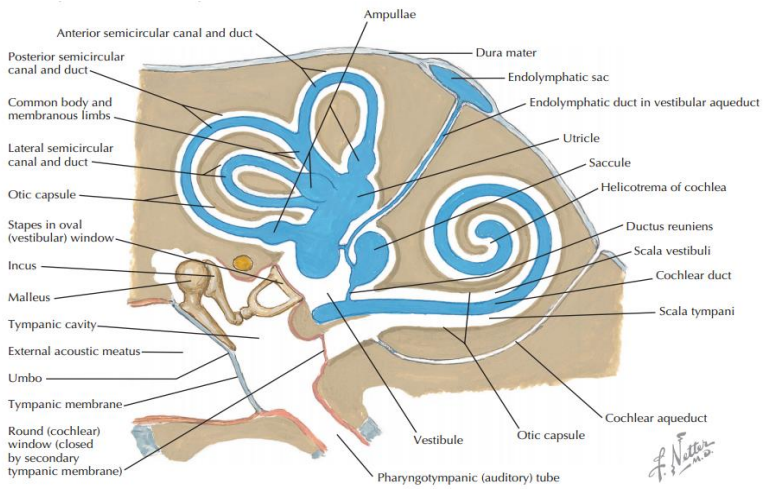

Figure 4. Representation of the bony (white) and membranous labyrinth (blue). Detailed illustration of the relation between the cochlea and the vestibular apparatus and its respective bony labyrinth. From (Felten et al., 2003).

The bony labyrinth is constituted by the cochlea, the vestibule and the semicircular canals (**Figure 4**). The cochlea, a spiral-shaped chamber, contains the Organ of Corti, which is the organ for audition. The bony labyrinth structures are filled with perilymph, a fluid that is alike and in continuance with the cerebral spinal fluid (Khan and Chang, 2013).

As it can be seen in **Figure 4**, although the membranous labyrinth (in blue) is quite smaller than the bony labyrinth (in white), they have equivalent forms except in the vestibule, where the membranous labyrinth acquires a sac-shape which makes up the utricle and saccule (Khan and Chang 2013). Additionally, endolymph, a fluid similar in composition to intracellular fluid, flows inside all the membranous labyrinth components (Mescher and Junqueira, 2013).

1.2.2. Hair cells

The vestibular system comprises mechanoreceptors named hair cells. They are specialized at the apical (or mechanical) pole as well as at their basal (or synaptic poles). From the apical surface emerges a single large kinocilium and several stereocilia (from 20 to approximately 100) (Goldberg and Oxford University Press., 2012). This stereocilia are arranged in rows of a descending fashion; from the biggest one (next to the kinocilium) to the smallest stereocilia. “Tip links” (represented in **Figure 5**) connect the tips of the shorter stereocilia to their neighbor (taller) ones (Barrett and Ganong, 2010). When head movements result in deflections towards or away from the kinocilium, the afferent nerve’s discharge will, respectively, be increased (excitation) or decreased (inhibition) (Goldberg and Oxford University Press., 2012).

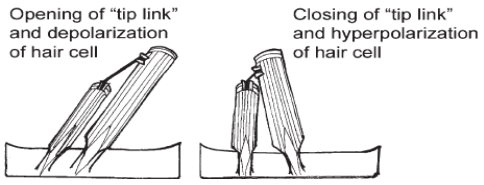

Figure 5. Schematic representation of hair cell’s “tip link” function. The bending of the kinocilium can either depolarize (increase of the “tip link” tension) or hyperpolarize (reduction of the “tip link” tension) the hair cell, releasing neurotransmitters that stimulate action potentials in the vestibular ganglion. From (Khan and Chang, 2013).

This hair cells constitute the sensory neuroepithelium of the crista ampullaris (located in the semicircular canals) and the macula (both utricular and saccular macula)(Khan and Chang, 2013).

1.2.3. Utricle and saccule

The utricle and saccule are able to detect linear acceleration, gravitational forces and tilting of the head (**Figure 6**A). Therefore, they give neural signs for coordination, position and movement of the head and neck. The utricle and saccule both have a sensory neuroepithelium named macula that can detect, respectively, motion in the horizontal or in the vertical plane (Khan and Chang, 2013). The maculae are bathed in a gelatinous membrane that buries small (3-30 μm in humans) particles of calcium carbonate ($CaCo_3$), the otoliths (Goldberg and Oxford University Press., 2012).

The stereocilia in the macula are oriented in respect to the striola (**Figure 6**B). The striola is a curvilinear line that is an area of thinning in the utricle and of thickening in the saccule. The hair cells are distributed towards the striola in the utricle and away from the striola in the saccule. This arrangement in different directions allows various patterns of hair cell stimulation depending on the direction of the head tilt (Khan and Chang, 2013).

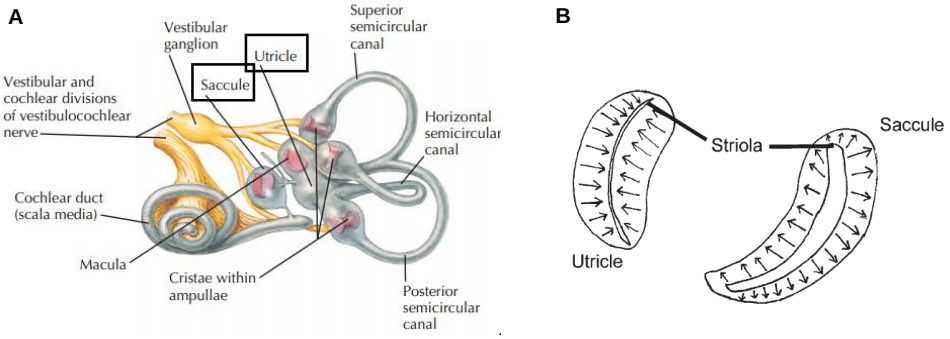

Figure 6. (A) Membranouslabyrinth. Utricle and saccule's position in the membranous labyrinth is highlighted with a black rectangle. Adapted from (Felten et al., 2003). (B) Schematic representation of the utricle and saccule and the relative location of the striola. Arrows represent the stereocilia in the macula, which are oriented in relation to each striola's profile. From (Khan and Chang, 2013)

1.2.4. Semicircular ducts

The three semicircular ducts have an equivalent format to the bony semicircular canals in which they are accommodated. They constitute the kinetic labyrinth which detects angular acceleration (rotation of the head, **Figure 7**A) and are arranged in the three orthogonal planes. The superior and posterior ducts are aligned 45º to the sagittal plane and the lateral canals are aligned 30º to the axial plane (**Figure 7**B). Contralateral semicircular ducts are mutually perpendicular and are paired with conjugate canals on the opposite side of the head organized as shown on **Table 1** (Khan and Chang, 2013). Hence, this 3-dimensional positioning enables each duct to sense movement a certain plane (Khan and Chang, 2013).

Table 1. The functional semicircular duct pairs. Adapted from (Khan and Chang, 2013).

Left horizontal	Right horizontal
Left anterior	Right posterior
Right anterior	Left posterior

Before the three semicircular canals open into the utricle, at each of their ends, exists a dilatation named ampulla. The ampulla contains the crista ampullaris, its sensory neuroepithelium, covered by the cupula, a gelatinous substance in which hair cells are embedded (**Figure 7**). Although the crista ampullaris is histologically similar to the macula, the cupula is thicker and doesn't have otoliths (Khan and Chang, 2013).

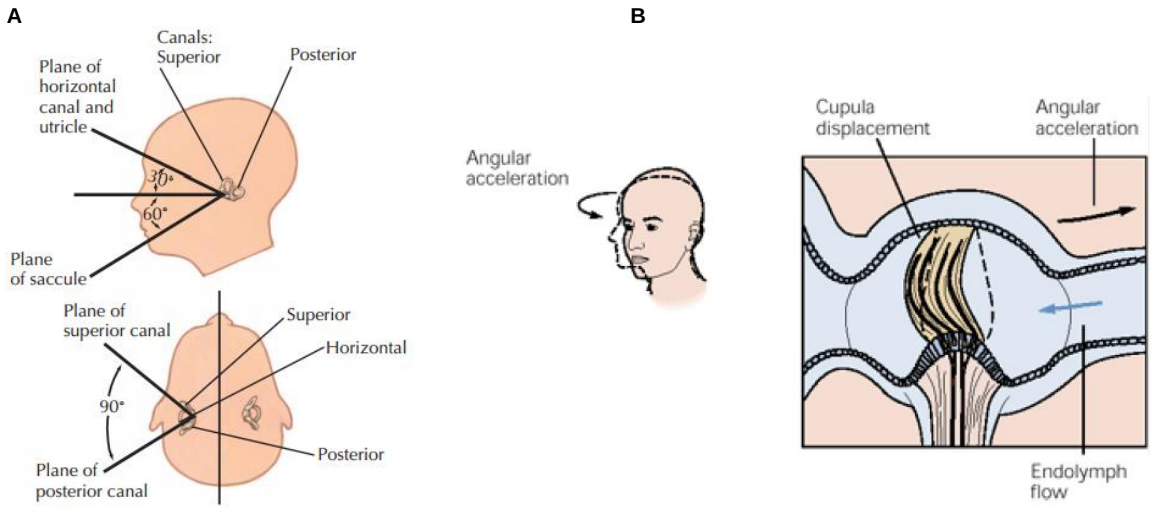

Figure 7. (A)Position within base of skull of the semicircular canals of the inner ear. The three semicircular canals are located at 90-degree angles to each other. From (Felten et al., 2003). (B) Left- Representation of the angular acceleration of a human head. Right - Ampulla of the semicircular ducts. Arrows indicate either head rotation (angular acceleration; black arrow) or the sense of the motion of the endolymph (blue arrow). The cupula is displaced by the flow of the endolymph when the head turns. From (Kandel, 2013).

1.2.5. Vestibular ganglion and vestibular nerve

In turn, the vestibular organs are connected to the vestibulocochlear nerve. It was Antonio Scarpa (1795), an Italian anatomist, who first accurately described the organs of the inner ear and their innervations (Wiest, 2015). The Scarpa's Ganglion (**Figure 8**), or vestibular ganglion, sits in the internal auditory meatus. It comprises, in humans, around 20.000 bipolar cell bodies that receive afferent impulses from the crista ampullaris (Adelman and Smith, 1999).

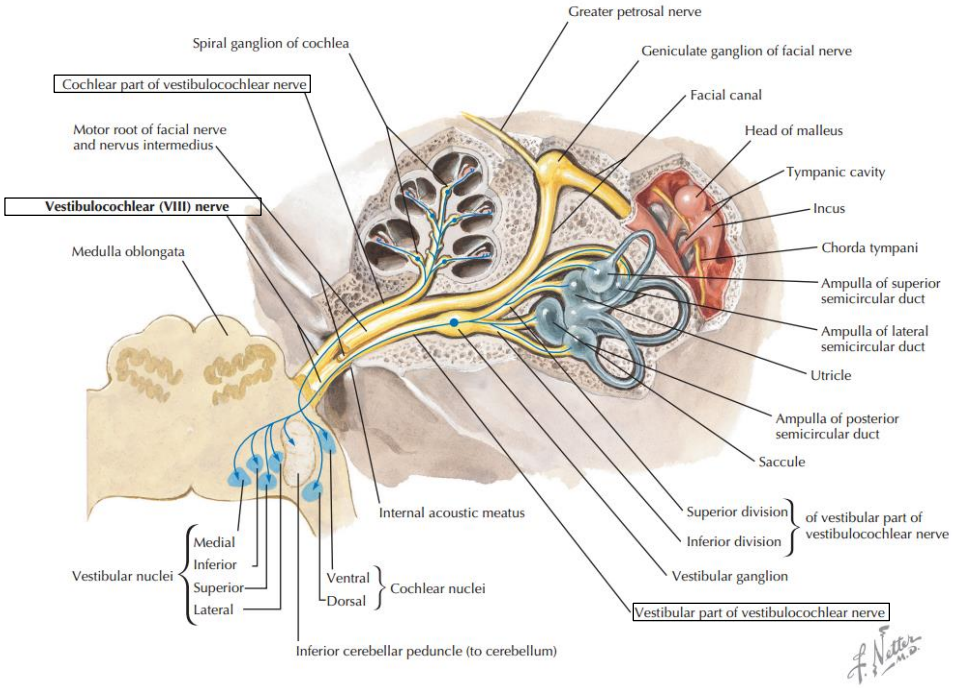

Figure 8. Anatomical representation of the vestibulocochlear nerve (VIII) (yellow). The vestibulocochlear nerve arises from the merging of the vestibular nerve with the cochlear nerve (structures indicated in black rectangles). The central processes of the vestibular ganglion cells terminate in vestibular nuclei (medial, lateral, superior, and inferior) in the medulla and pons and in the cerebellum. From Netter, 2016.

Axons from the vestibular ganglion merge to form the vestibular nerve. In turn, the vestibular nerve merges with the cochlear nerve to become the vestibulocochlear (VIIIth) nerve, disjoining again in the brainstem. The majority of the afferent fibers project to the ipsilateral vestibular nuclear complex in the pons (Khan and Chang 2013).

1.2.6. Vestibular nuclei complex

The vestibular complex is composed of four main nuclei: the superior (SVN), medial (MVN), lateral (LVN) and descending (DVN) (also called spinal or inferior) vestibular nuclei (**Figure 9**). The first three are also known as Bechterew, Schwalbe and Deiter respectively, named after their discoverers (Highstein and McCrea 1988). They are located under the floor of the fourth ventricle and go from the medulla to the pons in two major columns. The superior vestibular nucleus is located entirely in the pons. The medial vestibular nucleus is the largest of the four and composes the medial column. In turn, the lateral column is made up of the superior, lateral and inferior vestibular nuclei (Khan and Chang, 2013).

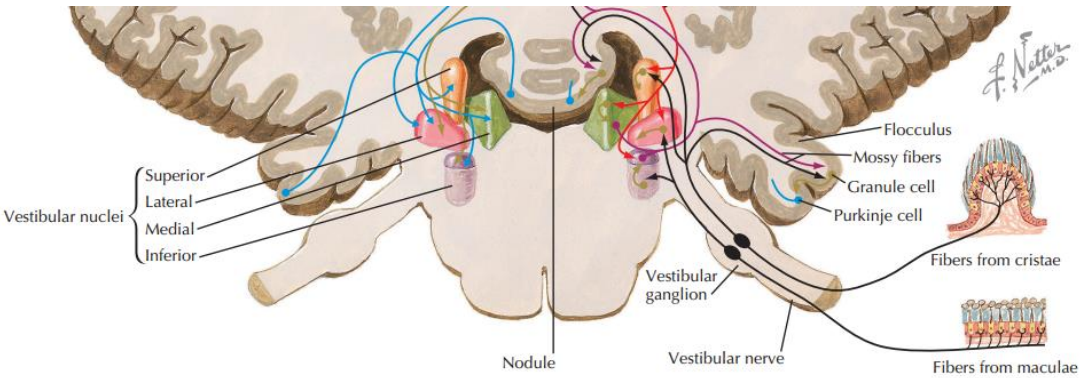

Figure 9. Vestibular nuclei complex. Colored lines represent the vestibular inputs terminations in the four vestibular nuclei: the superior (orange), the lateral (pink), the medial (green) and the inferior (violet). Adapted from (Felten et al., 2003).

Functionally, the vestibular nuclear complex is at the core of the circuitry responsible for processing and merging the input from the different vestibular organs with other non-vestibular information. Most of the vestibular-nerve afferents carry information and create convergences in the VN neurons (canal-canal, otolith-otolith and canal-otolith). Additionally, vestibulo-ocular (VOR) and vestibulo-colic (VCR, targets the neck to stabilize the head) reflex pathways arise in the VN. Both reflexes schematically depend on the integration of vestibular and visual or vestibular and proprioceptive information, respectively. Furthermore, mutual connections exist between the vestibular nuclei and the cerebellum. Due to its pivotal role in multisensory processing and in vestibular plasticity, its crucial to understand the characteristics of the central vestibular nuclei (Goldberg and Oxford University Press., 2012).

1.2.7. Central vestibular neurons

Central vestibular neurons (2ºVN) have an instrumental function in the processing of different sensory inputs (vestibular, visual and proprioceptive inputs). These neurons integrate these signals and generate a representation of the position and movement of the head-in-space which creates a pre-motor command used for gaze control (Beraneck and Idoux, 2012).

When functionally identified *in vivo*, 2°VN display various discharge properties (Shimazu and Precht, 1965, Precht and Shimazu, 1965). Based on their modulation during eye movements, 2°VN are classified into two main groups. One group is made of those that carry purely vestibular signals, the vestibular-only neurons (VO), most likely to mediate the vestibulo-spinal reflex (VSR) (Scudder and Fuchs, 1992, Roy and Cullen, 2001) and also project to higher brain areas (e.g., thalamus and cortex) to provide signals necessary for the sense of balance, orientation and navigation (Akbarian et al., 1988,

Buttner and Lang, 1979). Neurons in the second group of 2°VN carry eye movement related signals in addition to the vestibular signal. These neurons are directly involved in generation of the VOR (PVP, position-vestibular-pause neurons in monkey, or ES for Eye-Sensitive, in mice) (Beraneck and Cullen, 2007) or in VOR adaptation through inputs from the cerebellar flocculus (FTN, floccular target neurons)(Lisberger et al., 1994).

In vitro characterization of 2°VN neurons shows two groups of neurons: type A and type B in rodents or tonic and phasic in other vertebrates (Straka et al., 2005, Beraneck and Straka, 2011) (**Figure 10**A). These two types of neurons differ in their electrophysiological properties such as discharge dynamics (Straka et al., 2005), resonance frequencies (Ris et al., 2001), and neurotransmitter content (Takazawa et al., 2004, Bagnall et al., 2007). Current evidence regarding the putative roles of each subclass of 2°VN suggests that type A neurons are GABAergic neurons involved in local inhibitory networks (Shin et al., 2011) and a major component of the commissural system (Beraneck and Idoux, 2012, Bergquist et al., 2008). Type B neurons, either excitatory or inhibitory, are most likely the output neurons of the VN (Beraneck and Idoux, 2012)

How are these neurons categorized? 2°VN recorded on brainstem slices of mice (Dutia et al., 1995) and rats (Murphy and Du Lac, 2001) display pacemaker activity, which persists even when synaptic activity is reduced or blocked. The pacemaker activity of 2°VN in adult rodents is in the range of 15-30 spikes/s (Sun et al., 2002). Based on the resting discharge, researchers have focused their analysis on the electrophysiological signatures of the neurons (Beraneck and Idoux, 2012, Beraneck et al., 2004). Therefore, the type A/B classification doesn't relate to an anatomical scheme (connectivity) but rather to the neuron's electrophysiological features at rest (Beraneck et al. 2007).

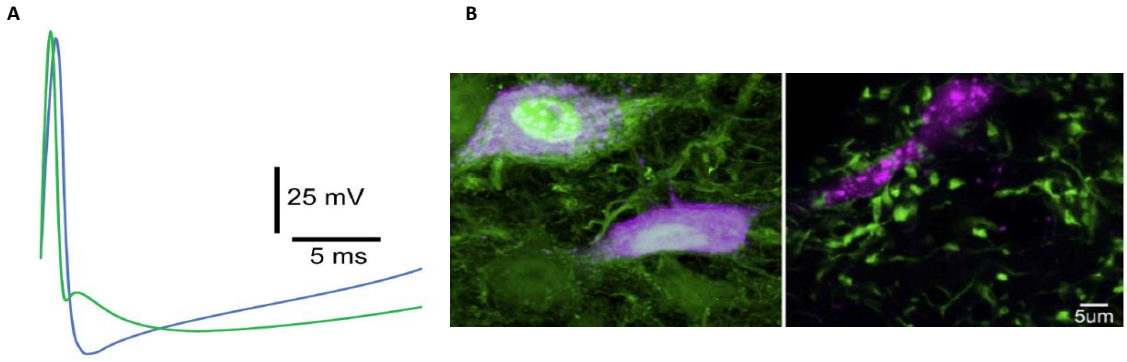

Figure 10. (A) Static properties of MVN neurons. Superimposed spike traces of type A (blue) and Type B (green). From (Beraneck and Idoux, 2012). (B) Images of the MVN neurons of two transgenic lines. Left- YFP-16 mouse line; neurons expressing fluorescent protein in (green) and retrogradely labed with stereotaxic dye injection (purple). Right- GIN mouse line; neurons are labeled in green and the dendrites of a neuron in purple. From (McElvain et al., 2010).

Hence, the classification into type A and type B is based on the shape of their action potential, the subsequent after hyperpolarization (AHP) and interspike intervals (Serafin et al., 1991, Eugene et al., 2011). Type A neurons have a single and deep AHP followed by an inflection that retards the depolarization of the neuron (I_A-like rectification). On the other hand, type B neurons show a first fast AHP followed by a slow one, therefore they have a so-called biphasic or double AHP (dAHP). Quantitatively, mice aged approximately 30 days, possess 70–80% type B neurons and 20–30% type A neurons (Eugene et al. 2007).

Both types of neurons are differently inserted in the vestibular networks since most type A neurons, based on their neurotransmitter content, seem to be GABAergic while type B could be glutamatergic or glycinergic (Takazawa et al. 2004). Hence, the type A neurons correspond to tonic cells involved in inhibitory network. Type B neurons are the phasico-tonic excitatory or inhibitory output of the vestibular network (Biesdorf et al. 2008, Rossert and Straka 2011).

As mentioned, the neurotransmitter content of MVN neurons also enabled to distinguish two main categories. For this purpose, two transgenic mouse lines were used: GIN line expressing green fluorescent protein in inhibitory GABAergic neurons and YFP-16 line expressing yellow fluorescent protein in non-GABAergic (glycinergic or glutamatergic) (McElvain et al. 2010; Shin et al. 2011) (**Figure 10**B).

Although the two mentioned distributions (Type A/B and GIN/YFP) are not strictly equivalent, based on their action potential profiles, GIN would correspond to type A and YFP to type B neurons (Eugene et al. 2011).

1.2.8. Extraocular muscles

In turn, emerging from the brainstem, the cranial nerves will innervate the extrinsic muscles of the eye. For the eyes to be able to execute their movements, the extraocular muscles (EOMs) are innervated by three groups of motor neurons whose cell bodies form the nuclei in the brainstem shown in **Figure 11**.

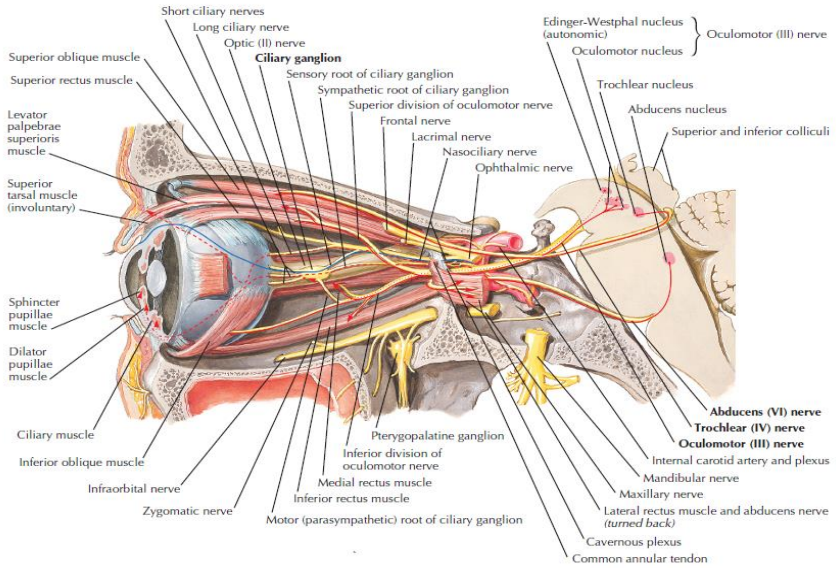

Figure 11. Cranial nerves and their nucleus and nerves of the orbit nerves. The abducens nucleus (VI) is located in the pons. The oculomotor nucleus (III) is in the midbrain, adjacent to the trochlear nucleus (IV). From (Felten et al., 2003).

The lateral rectus is innervated by the abducens nerve (cranial nerve VI); the superior oblique is innervated by the trochlear nerve (cranial nerve IV); the medial, inferior and superior recti and inferior oblique muscles are innervated by the oculomotor nerve (cranial nerve III)(Felten et al., 2003).

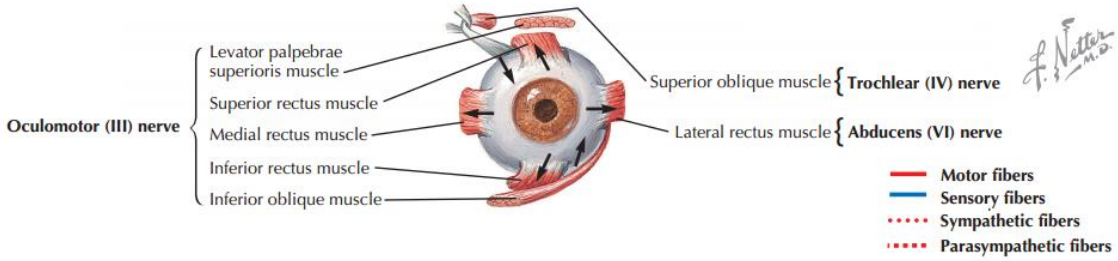

Figure 12. The global position of the EOMS. The orbital wall is not represented in order to give a clear frontal view of the eye. The VI cranial nerve (CN) innervates the lateral rectus muscle; the IV CN innervates the superior oblique muscle; and the III CN (oculomotor nuclei) innervates the medial rectus, superior rectus, inferior rectus, and inferior oblique muscles. From (Felten et al., 2003).

Consequently, the six existing EOMs will control the turning of the eyes (represented in **Figure 12**) and they are arranged in three antagonistic pairs. The lateral and medial recti muscles control the side (left-right) rotation. The superior and inferior recti muscles control up and down eye movements. The superior and inferior oblique muscles control the torsional rotation and elevation of the eye (Kandel, 2013).

2. Gaze stabilizing reflexes

Raymon Dodge, in the early 90's, was responsible for the classification of the eye movements, that are used to project or stabilize gaze, into five groups. Three of them are voluntarily initiated movements to direct gaze to a particular object in the visual field: saccades (a scanning motion, rapid discontinuous), smooth pursuit (to track small moving targets) and vergence (to move the eyes in two different angles so that they converge on near or far targets) (Goldberg and Oxford University Press., 2012). The two other classes of eye movements – the vestibulo-ocular reflex (VOR) and optokinetic reflex (OKR) – are reflexes that function to hold images stationary on the retina, a pre-requisite to vision. These two crucial reflexes work daily together to stabilize gaze (eye-in-space) during head motion (**Figure 13**).

Contrarily to VOR, the OKR relies on visual inputs instead of vestibular ones to stabilize gaze. Independently of head movement, OKR is commanded by the relative movement of the spatial context (visual field) across the retina. OKR stabilizes vision mainly at low-frequencies while VOR functions at higher frequencies (Faulstich et al., 2006). The OKR creates an eye movement which consists of alternating slow (smooth pursuit) compensatory in one direction and quick (saccadic) retuning eye movements on the other direction (Goldberg and Oxford University Press., 2012).

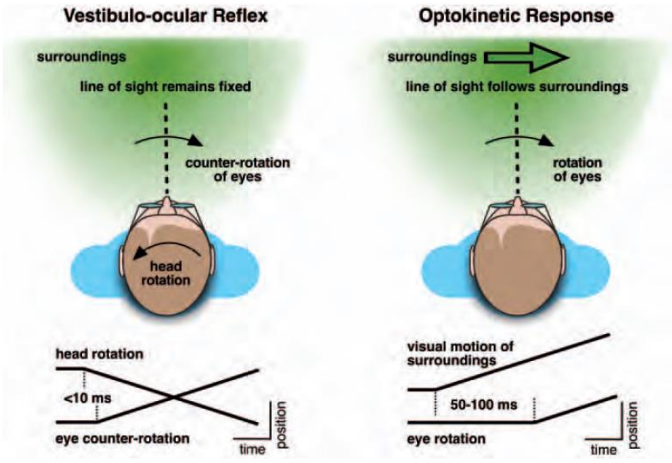

Figure 13. VOR and OKR, eye movements that stabilize gaze. Left - The VOR counter-rotates the eyes during head movements, maintaining the image stable in the retina. The eyes rotate right after the start of the rotation of the head. Right - The OKR, after longer latency, stabilizes the line of sight with respect to the moving visual environment. From (Squire, 2003).

2.1. The vestibulo ocular reflex (VOR)

The vestibulo ocular reflex (VOR) consists in automatic eye movements that stabilize the eye-in-space position by directing the eye in the opposite direction of the head movements (**Figure 14**). The VOR produces eye movements in response to both horizontal (HVOR) and vertical (VVOR) head rotations (Boyden et al., 2004). The vestibulo-ocular reflex is often described as a very rapid, 3 neuron-reflex-arc (see description below in 2.2). The VOR response can be as short as 5-10ms which makes it one of the most rapid sensorimotor chain of the brain (Goldberg and Oxford University Press., 2012).

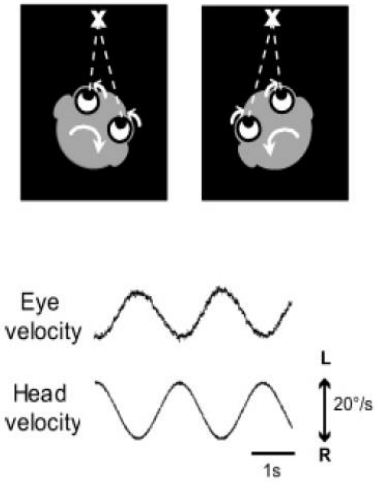

Figure 14. Vestibulo-ocular reflex - Eyes move in the opposite direction as the head. This results in the eyes being stationary in respect to the surroundings. From (Boyden et al., 2004).

Although its function is to provide clear vision by stabilizing gaze, the VOR is experimentally measured in the absence of light so that the eye movements driven by vestibular stimuli are isolated from eye movements driven by visual stimuli. It is important to state that, this reflex works as an open-loop that doesn't depend on visual input. That is, it works even in the absence of image in the retina because its visual system feedback is not essentially part of the reflex. However, the calibration of the reflex does depend on the visual feedback through essentially the same pathway as the OKR pathway (Accessory optic system; nucleus of the optic tract; inferior olive; cerebellum).

The performance of the VOR is characterized by the gain – ratio between eye and head velocities – and phase – i.e. the temporal relationship between eye and head movement (Broussard and Kassardjian 2004). Consequently, a perfect VOR would have eye movements of equivalent magnitude to the head movements, generating a gain of 1.0 and beginning at exactly the same moment as the head movement, with a phase of 0º (Blazquez et al., 2004).

Experimentally, the VOR possesses numerous advantages that make it an adequate model to study motor learning: it can be tested with easily controlled sensory inputs, it has quantifiable motor outputs, a fairly well described circuit anatomy and precise quantification methods (Boyden et al., 2004, Blazquez et al., 2004). Until early 2000s, VOR adaptation studies have been dominated by the Human and rhesus monkey models. It is only with the apparition of video-oculography that mice were shown to have a perfect VOR (Stahl, 2004). Since then, a growing body of evidence emerge from laboratories which have taken advantage of the genetic tools available in mice.

2.2. The horizontal vestibulo-ocular pathway

This reflex is really fast and relatively simple as it comprises a three neuron arc sensorimotor pathway; from the vestibular afferents, to the vestibular nuclei, and after to the ocular motor neuron to enable eye motion in an equal but oppositely direct movement of the head (Blazquez et al. 2004). For explanatory purposes, we will consider a VOR of the eyes to the right, in compensation of a head rotation to the left (**Figure 15**). The rotational acceleration of the head turning left causes endolymph flow in the ampulla, deflection of the cupula and hair cells to the right side. Consequently, this bending will cause the opening of the ion channels and depolarization of the hair cells. This mechanotransduction transformes a movement into a neural signal which increases the firing of the vestibular afferent fibers from the left side of the head. The opposite will occur on the contralateral (right, in this case) hair cells, causing hyperpolarization (inhibition) and a decrease of the right afferents discharge. Passing through Scarpa's ganglion, the firing frequency of the VIIIth nerve in turn will increase and impulses will be sent mainly to the ipsilateral superior and medial vestibular nuclei through first-order vestibular neurons (1º VNs, which axons constitute the VIIIth nerve). Excitatory/inhibitory impulses are in turn sent to the contralatreral/ipsilateral abducens nucleus (VIth nerve) through neurons in the right/left vestibular nucleus (VN), respectively. Internuclear neurons in the abducens nuclei cross the midline and ascend to the MLF to terminate on the contralateral medial rectus motorneurons (oculomotor, IIIth nerve). Thus, motor neurons on the right VI nuclei and left III nuclei fire at a higher frequency, while those on the left VI and right III fire at a lower frequency. This will cause a contraction of the right lateral rectus and left medial rectus and the distention of the right medial rectus and left lateral rectus, resulting in both eyes moving to the right (or contrary to head turning) (Goldberg and Oxford University Press., 2012).

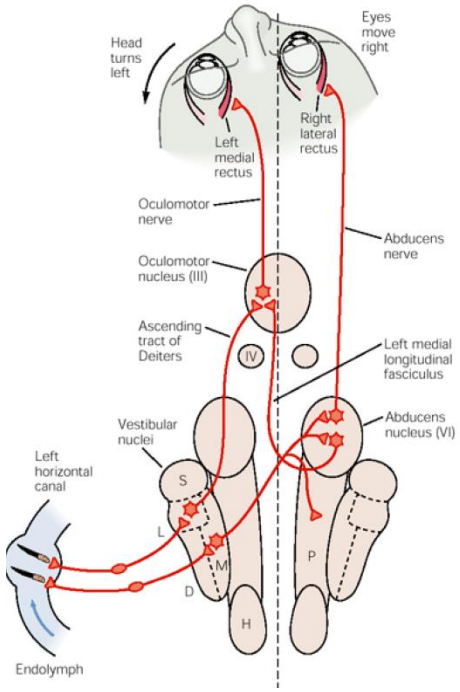

Figure 15. Head rotation to the left and associated VOR pathway. Excitatory connections of the head turning to the left which cause eyes to move to the right. (M) medial vestibular nucleus; (L) lateral vestibular nucleus; (D) descending vestibular nuclei; (S) superior vestibular nuclei; (P) prepositus hypoglossi; (H) nucleus prepositus hypoglossi; (III) oculomotor nucleus; (IV) trochlear nucleus; (VI) abducens nucleus. From (Kandel, 2013).

When the head stops turning (rotational velocity constant), the cupula returns to its upright position, regularizing the membrane potential of the hair cells and reducing the afferent nerve fibers (Khan and Chang, 2013).

3. VOR adaptation

As previously mentioned, although the VOR functions in the dark, its calibration depends on the presence of visual stimuli in which normally, the eye movement locks the eye perfectly to the visual scene. When there is a mismatch between the visual and vestibular information, the image of the object moves on the retina, causing a blurred vision. This event is called retinal slip. In result to this error signal, which says that eye movements are not being compensatory, there is motor learning to adjust the gain of the VOR to give an improved eye motion. The process of motor learning modulation in order to restore gaze stabilization is called VOR adaptation. VOR adaptation is tremendously needed through life since neurons and muscles grow, deteriorate and eventually die (Broussard and Kassardjian 2004). Also, in humans the VOR needs to be constantly adjusts since young age in order to accompany the changes in head circumference (Goldberg and Oxford University Press., 2012). This adaptation to new conditions is possible through

motor learning in the VOR, which is caused by persistent image motion during head movements, resulting in the increase or decrease of the gain.

Experimentally, it is possible to create motor learning in laboratorial conditions through the pairing of image motion with head motion. Depending on the relative direction of the head motion and image motion, the gain of the VOR can be adaptively increased or decreased, as shown in **Figure 16**. A gain-up stimulus results in an increase of the VOR gain and is obtained by training with image motion in the opposite direction opposite that of the head (increase in retinal slip). A gain-down stimulus decreases VOR gain and, is induced by image motion in the same direction as the head (decrease in retinal slip; Boyden et al. 2004).

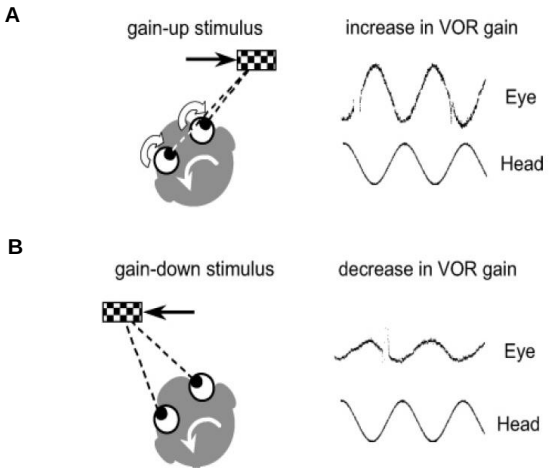

Figure 16. Motor learning in the VOR. (A) Gain up stimulus: the increase in VOR gain is achieved by training with an image (chess box, in this case) movement in the opposite direction of the head. (B) Gain down stimulus: the decrease in VOR gain is achieved by training with the image (chess box) movement in the same of the direction of the head. Adapted from (Boyden et al., 2004).

A common example to describe this adaptive plasticity is a subject putting on a newly prescribed pair of eyeglasses. The adaptation to the optical magnification needs the recalibration or plasticity of the VOR. If the magnification is augmented, a movement of the head will result in a bigger and quicker movement of the image across the retina and will obtain an increase of the VOR in order to maintain stability. In turn, a decrease in the augmentation would translate in VOR gain decrease (Goldberg and Oxford University Press., 2012).

3.1. Possible sites of motor learning

Motor learning can be defined as the process that improves the smoothness and accuracy of movements (Boyden et al. 2004). It is required for intricate movements (for example, playing the saxophone) but also for calibrating simple sensorimotor chains like the VOR. It is known that the cerebellum is critical for motor learning (Boyden et al. 2004) and two long-standing hypotheses provide two very different accounts about the role of the cerebellum for motor learning in the VOR. Essentially, the difference between these two models is the location of the modified synapses that underlie motor learning (**Figure 17**).

Even before VOR plasticity was demonstrated, Ito (Ito, 1972) proposed a theory based on the Marr-Albus hypothesis of cerebellar motor learning (Albus 1971, Marr 1969). Ito theorized that the role of the cerebellum is to store the motor memory for the learned change in VOR gain. More specifically, the climbing fibers (CF) input from the inferior olive provide an error signal in response to the retinal slip, that would cause long-term depression (LTD) at the synapses between parallel fibers and Purkinje cells which would alter the efficacy of these synapses. This synaptic plasticity would then modify the activity of vestibular nuclear neurons and thus change the gain of the VOR. Consistent with this theory is the fact that floccular complex (located in the cerebellum) is essential for the acquisition of VOR plastic changes (Rambold et al., 2002) and CF inputs to the floccular complex encode retinal slip. Therefore, according to Ito's framework, learning would continue until the signal encoded by the climbing fibers becomes zero. At this point the VOR becomes completely compensatory and no more adaptation is needed.

Few years later, an alternative model was proposed by Miles & Lisberger (Miles and Lisberger, 1981). The authors proposed that the role of the cerebellum was not to store the motor memory but to provide a teaching signal guiding the induction of plasticity in the brainstem.

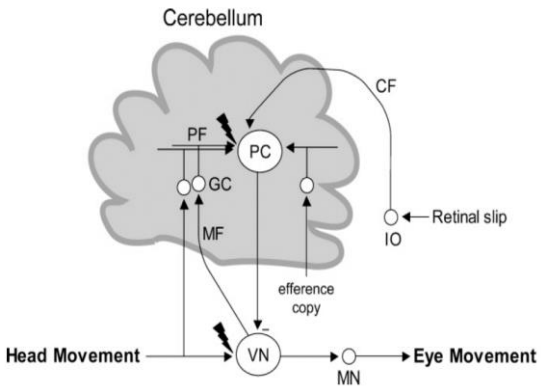

Figure 17. The two different locals (indicated by the black lightning bolts) of plasticity proposed by Ito's hypothesis and Miles&Liberger hypothesis. CF, climbing fibers; GC, granule cells; IO, inferior olive; MF, mossy fibers; MN, oculomotor nuclei; PC, Purkinje cells; PF, parallel fibers; VN, vestibular nuclei. Adapted from (Boyden et al. 2004)

3.1.2. Brainstem plasticity after long-term VOR adaptation

Initially, support for the brainstem hypothesis mainly came from experiments that evaluated alterations in Purkinje cells (Boyden et al. 2004). It was found that changes in the VN neurons could not be accounted for the input received by Purkinje cells so, they must be a consequence from plasticity events somewhere outside the cerebellum (Lisberger, 1994).

However, VOR adaptation can be short-term or long-term. Long-term adaptation, is achieved over a longer period of time (usually more than a week) and, unlike short-term adaptation, it creates persistent alterations within the oculomotor circuitry.

Later on, studies focused on experiments using cerebellum deactivation, which verified that flocculi shutdown suppresses VOR short-term, but not long-term adaptation. The short-term storage of adaptive memories in the cerebellum has been confirmed also by OKR experiments. The memory trace of short-term OKR adaptation seems to be encoded and initially to reside in the flocculus, while long-term adaptation is probably achieved by the transfer of this memory to the vestibular nuclei (Shutoh et al. 2006, Anzai et al. 2010, Okamoto et al. 2011).

Although the hypothesis of a long-term retention of adaptive memory in the brainstem has been suggested and given support from several theoretical studies as seen in **Figure 18** (Yamazaki et al., 2015, Clopath et al., 2014, Menzies et al., 2010, Masuda and Amari, 2008, Porrill and Dean, 2007), it doesn't have yet any experimental support *in vitro*, and the underlying mechanisms therefore remain elusive.

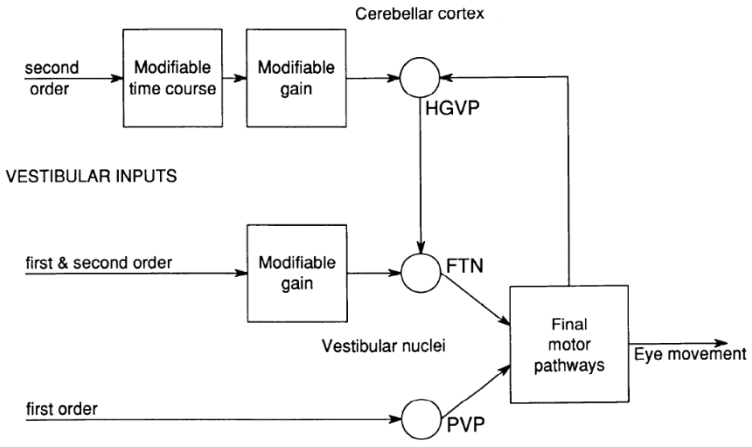

Figure 18. A hypothesis of motor learning in the VOR. The vestibular inputs come from the left (head velocity) and the motor outputs are represented on the right (eye movement). The eye velocity positive feedback pathway is the loop from HGVP to FTN to the "final motor pathways" square. The circles indicate the summing junctions HGVP horizontal gaze-velocity Purkinje cell; FTN, flocculus target neuron; PVP, position-vestibular-pause neuron. From (Lisberger, 1994).

4. Aims of the project

The goal of the project is to investigate, in the mouse model, the question of the long-term retention of VOR motor learning in the brainstem. The design of the experiment is to allow a system approach with combination of *in vivo* and *in vitro*.

To investigate this question, I performed an *in vivo* innovative VOR long-term adaptation protocol, developed by my team, which exposes mice to a visuo-vestibular mismatch (VVM) for 14 days leading to VOR long-term adaptation. A combination of *in vitro* electrophysiological experiments, immunohistochemistry, use of genetically-engineered mice lines and VOR measurements were executed. By performing whole-cell patch-clamp experiments in brainstem slices, we aimed to understand the neuronal changes that occur after the 14 days of VOR adaptation. Immunohistochemistry was performed to explore the expression of the receptors involved in synaptic transmission. Finally, using VOR measurements, we tested the influence of the retinal slip on the VOR adaptation and the retention of this memory using this new behavioral adaptation protocol.

Materials and Methods

1. Animals

Male C57BL/6J WT (Janvier, Le Genest Saint Isle, France) and 3 transgenic lines GAD67-GFP, Pvalb-Cre (Hippenmeyer, Vrieseling et al. 2005) and Sst-Cre (Taniguchi, He et al. 2011) were used for the experiments hereafter described. All animals were housed with the cycle of 12h light/12h dark and fed with standard rodent chow and water *ad libitum*. The weight and well-being of every mice was tracked daily (a record sheet of the weight for one group is available in **Annex 1**). Animals were used in accordance with the European Communities Council Directive 2010/63/EU and all the procedures were approved by the ethical committee for animal research of the University Paris Descartes 34 (CEEA.34).

2. Visuo-vestibular mismatch protocol

2.1. Headpost implantation surgery

Animals were anesthetized with isoflurane gas (Iso-Vet, Ireland). The head was shaved using an electric razor. A longitudinal incision of about 2 cm was performed in the skin to expose the skull. Then, a customized headpost (size: 3.0mm width x 1.5mm depth x 3.0mm height; weight 0.3g) was cemented (Super-Bond C&B, Sun Medical, Japan) to the skull between lambda and bregma landmarks. A small RFID (Radio-Frequency IDentificatiion) chip was inserted subcutaneously to allow the identification of each mouse. In order to ensure a painless healing, 0.1mL of lidocaine (Xylovet, France) and 0.1mL of Vetedine® (Vetoquinol, France) were applied on top of the suture area.

Following the surgery, the animals were placed under a red light to avoid hypotermia and with buprenorphine 0.05mg/kg diluted in the water to ensure postoperative analgesia. As soon as the mice woke up and started moving comfortably, they were placed in cages in the respective groups of 3 or 4 animals to stimulate social interactions. Images of the surgical procedure are on **Annex 2**.

2.2. Adaptation device

Two to three days following the surgery, a custom-built helmet (size: 2.2mm width x 1.5mm depth x 1.5mm length; weight 3g) was secured onto the headpost of the mice. This device covers almost completely the face of the mouse while respecting the facial

anatomy of the animal in order to prevent the blockade of the nose and to allow the animal to eat and drink normally (see **Figure 19**).

Two types of helmets were used: translucid or striped. The translucid devices were made of translucent plastic so that light can reach the eye but no coherent image can be seen through it. The striped helmet was made of translucid plastic with additional 3mm-thick black stripes drawn along with a permanent marker. Using the striped helmet, the animal sees a high contrast, fixed visual signal during self-generated head movements. The use of these two different devices served the purpose to study the effect of the retinal slip on the adaptation of the VOR. When the animal moves and performs VOR, the striped device induces a retinal slip, as the image on the retina (black stripes) is fixed. On the other hand, the use of the translucid device causes the mouse to see no coherent image, which hypothetically reduces the retinal slip error signal on the retina.

Figure 19. Images of the striped device used for inducing VOR adaptation. The mouse is wearing a helmet, made of translucent plastic with vertical black stripes drawn on the surface which completely covers the mouse's head

2.3. Adaptation protocol

In the first few hours after the implantation of the device, mice exhibited a troubled behavior with difficulties to orientate in the cage, often bumping into the walls leading to a reduction in social interactions. They also showed problems to properly reach for food and water and therefore received extra attention during the first 24h. After 2 days, general behavior was restored to normal with perfect orientation in the cage, normal locomotion and normal social interactions.

At the end of the adaptation protocol, after 14 days with the device on, mice either performed behavioral experiments (video-oculography measures) or were used for *in vitro* electrophysiology experiments or for immunohistochemistry experiments. Regarding the electrophysiology and immunohistochemistry experiments, only mice adapted with the striped helmet and mice which did not wear any device (i.e. controls) were used.

3. Electrophysiological experiment

The neural changes following VOR long-term adaptation were studied using whole-cell patch clamp electrophysiology, on both control mice and mice following VOR adaptation. Recordings were performed in the medial vestibular nucleus (MVN) which encodes sensorimotor vestibular transformations in the horizontal plane.

3.1. Slice preparation/dissection

Adult mice, 35-38 days old, either control or following VOR adaptation, were deeply anesthetized by intraperitoneal injection of pentobarbital (5 mL/Kg) and, after ensuring deep anesthesia, quickly decapitated. The brain was then removed and placed in ice-cold phosphate/bicarbonate-buffered artificial cerebro-spinal fluid solution (25 mM $NaHCO_3$, 1mM NaH_2PO_4, 2.5 mM KCl, 3 mM $MgCl_2$, 10 mM Glucose, and 240 mM sucrose oxygenated with 95% O_2 / 5% CO_2). First, an incision was made in the skin longitudinally across the head, and the frontal and parietal bones were removed. A cut rostrally to the cerebellum at a +15º angle was made in order to optimize the preservation of the afferent fibers in the slicing plane. Coronal brainstem slices of 300µm were cut, using the same ACSF solution, on a vibratome (Leica VT100S, Germany) and transferred into an incubating vial filled with a regular ACSF (recording solution) containing 120 mM NaCl, 25 mM $NaHCO_3$, 1 mM NaH_2PO_4, 2.5 mM KCl, 2 mM $MgCl_2$, 10mM Glucose and 1 mM $CaCl_2$, oxygenated with 95% O2 / 5% CO2 gas mixture in order to maintain the physiological pH 7.4, during approximately 1.5h before the beginning of the recordings. Slices were then placed in the recording chamber maintained at 32-34°C and superfused with regular ACSF at a constant flow rate of 3 mL/min.

3.2. Whole-cell patch clamp recording protocol

The recording solution was perfused into the recording chamber using a peristaltic pump. The neurons were visualized with a fixed-stage upright microscope (BX51WI, Olympus) using differential interference contrast illumination with Nomarski optics, mounted onto an anti-vibrating table (TMC, USA). The image obtained was processed by a camera controller (C2741-63, Hamamatsu, Japan). A high-precision electric micromanipulator (MPC-200, Sutter Instruments Company, USA) was used to move the recording electrode. The temperature of the recording chamber was kept between 33-35ºC with a dual automatic temperature controller (TC-344B, Warner Instrument Corporation, USA) (Picture of the experimental set up in the Annexes).

Recordings were made using a clamp headstage (CV-7B, Axon Instruments, Foster City, CA), filtered by a low-pass filter (Model 3900, Krohn-Hite Corporation), transferred to the amplifier Multiclamp 700B (Molecular Devices, Sunnyvale, CA, USA). Current and voltage from the amplifier were low-pass filtered at 2 kHz and digitized at 5 kHz (BNC- 2090 + PCI-6052E, National Instruments, Austin, TX, USA). The signal was then transmitted to a computer (HP, Windows operative system) running the data acquisition and analysis software Multiclamp® (Molecular Devices, USA) and Matlab (MathWorks, Inc).

The patch pipettes were made of borosilicate glass (GC150F-15, Clark Electromedical) with an outer diameter of 1.5 mm and were pulled by a horizontal micropipette puller (P-2000, Sutter Instruments Company, USA). The open tip resistances ranged between 4-8 MΩ. The internal solution (Sekirnjak and du Lac 2006) contained 140 mM Kgluconate, 5 mM KCl, 10 mM Nafree-HEPES, 0.1 mM EGTA, 2 mM $MgCl_2$, 0.03 $CaCl_2$, 4 Na_2- ATP, 0.4 mM Na_2-GTP; osmolarity adjusted to 300mOsm with K-gluconate. Whole-cell patch clamp recordings were mainly performed in medium-large sized neurons of the medial vestibular nucleus on control mice and on mice following VOR adaptation (after 14 days with the striped helmet).

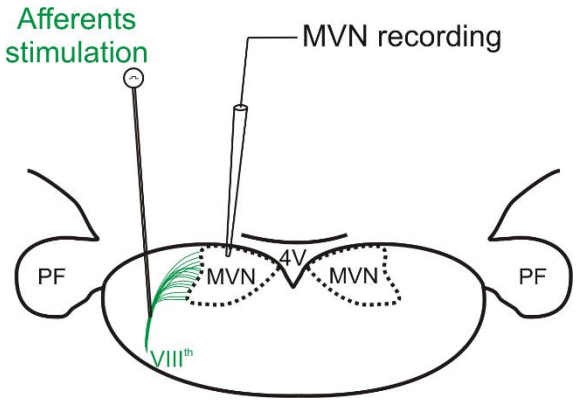

Figure 20. Illustration of in vitro patch-clamp recordings of medial vestibular nucleus (MVN) neurons on coronal brainstem slice. A bipolar electrode is used to stimulate the vestibular afferents en passant. PF: Paraflocculus regions; 4V: 4th ventricle.

After the surface of soma of a neuron was approached with a pipette, suction was applied until a gigaohm seal was made. All neurons were patched in current clamp mode and a protocol was applied to study their static and dynamic properties. The routines were written in Matlab (The Mathwork).

After the successful patching of a neuron, a first spontaneous discharge recording was made (~ 3 minutes) along with some hyperpolarizing steps (-20, -40 and -60 pA) until a stable membrane potential of about -60mV was reached. To minimize variability linked to local inhibition, the GABAergic receptors were blocked using Picrotoxin (1mM)

and the glycinergic receptors using Strychnine (1mM). A second spontaneous recording was performed with the addition of these inhibitors. Following, a first stimulation of hyperpolarizing and depolarizing steps (from -130pA to 130pA) was performed. Then the neuron was switched to voltage clamp mode (potential holding of -70mV), and first a new spontaneous discharge recording was performed. Then a new stimulation using hyperpolarizing and depolarizing steps (±20mV) was performed at different holding potentials: -70mV, -40mV and -10mV.

On all patched neurons, an attempt was made to stimulate the vestibular afferents by positioning a bipolar concentric electrode on the vestibular nerve (CBAPC75, FHC, USA). The placement of the electrode was favored at the top of the nerve, where the fibers start to spread, around 6 - 6.4 mm caudal to bregma, 4.4 mm ventral to the horizontal plane passing through bregma and lambda, and 1.7 - 1.8 mm lateral to the midline. The intensity of the stimulation applied with the electrode ranged from 270pA to 310 pA in order to achieve the biggest eEPSC amplitude. On some neurons (31 control and 17 adapted), evoked EPSCs (eEPSCs) were measured every 15 seconds while holding the cell at different potential (-70mV, -50mV, -30mV, -10mV, 10mV, 30mV, 50mV).

3.3. Data analysis

Basic and firing properties of MVN neurons were recorded (Eugene et al. 2007) and analyzed using custom-made Matlab software (The Mathwork).

Static properties of MVN neurons

Using the spontaneous discharge recordings for each neuron, the potential was low-pass filtered at 1 Hz to obtain an estimate of its average resting level that was taken as the “mean resting membrane potential” (Vm in mV) of each neuron. Since MVN neurons are spontaneously active on slices, the average of the spike shapes and inter-spike interval profiles were measured in order to obtain the spontaneous firing rate (spikes/s), the amplitude of the after-hyperpolarization (AHP in mV), the double amplitude of the after-hyperpolarization (dAHPR in mV), the spike threshold potential (in mV) and the concavity and convexity (in mV) of the inter-spike interval.

Neurons were classified as type A or type B as described in (Beraneck, et al. 2003, **Table 2**):

Table 2. Type A and type B classification parameters. Adapted from (Beraneck et al., 2003).

	dAHPR (mV)	
AHPR (mV)	0	>0
<0.08	B	B
>0.08	A	B

Dynamic properties of MVN neurons

Active membrane properties were analyzed using the steps experiments and compared between adapted and control mice. This stimulation in current-clamp mode allowed to create current/frequency (I/F) curves and to estimate the excitability of the neurons. The same stimulation in voltage-clamp mode permitted to create current/voltage (I/V) curves to study the impact of adaptation on the conductance of the neurons. The analysis of the eEPCS allowed assessing synaptic efficiency by measuring their amplitude (pA), the area under the curve (AUC, fC) and time constant (τau, ms).

4. Immunohistochemistry

4.1. Immunohistochemistry protocol

Since the synaptic transmission between the vestibular afferent and the vestibular neurons is mainly an excitatory glutamatergic transmission through NMDA and AMPA receptors, immunohistochemistry was performed to target these receptors in the MVN using both control mice and mice adapted with the striped helmet.

In total, 8 adapted and 9 control mice of 35 days old were used. Mice were deeply anaesthetized by an intraperitoneal injection of Pentobarbital (5 mL/kg). They were then intracardiacally perfused with phosphate-buffered saline (PBS, 0.1M) followed by 4% paraformaldehyde (PFA) fixative, and the brains were carefully removed and placed in PFA for 24h. Brains were then placed in sucrose solution (30%) for at least 48h.

Brain slices (80 µm) were cut in a freezing-slide microtome and were immediately placed in PBS 0.1M. The free-floating coronal serial brainstem sections were immediately post-fixed in PBS 0.1M for 3 washes of 10 minutes each. During each step, the sections were agitated on a rotator at room temperature (25ºC). Slices were then preincubated with blocking solution (20 mL PBS, 1000 µL normal goat serum (NGS) corresponding to PBS-NGS 5%) for 1 hour. Slices were then washed two times during 10 minutes and for a final step during 1h30 with PBS-NGS 1%. For each mouse, 2 brain

slices containing MVN were used to perform NMDAR2 staining, 2 slices for AMPA staining (GluR2/3) and 2 last slices for non-specific staining (without any primary antibody).

First, slices were incubated with 400 µL of primary antibodies diluted at appropriate concentrations (1:50 Anti-NMDAR2a/b; 1:50 Anti-AMPA; AB1548 and AB1506, respectively, rabbit polyclonal antibodies- Merck Millipore, Germany) and were left overnight at room temperature (RT) in constant rotation. Sections were then washed two times with PBS-NGS 1% for ten minutes and one time for 30 minutes. This step was followed by the incubation with the secondary antibody (goat anti-rabbit IgG secondary antibody, Alexa Fluor™ 546 conjugate – ref A11010, Life technologies, USA) during 1h30 at RT. After two washes in PBS 0.1M, a third wash of ten minutes was made using 1µg/mL 4',6-diamidino-2-phenylindole (DAPI) (D1306, ThermoFisher Scientific, USA) in 0.1 M PBS. Finally, the resulting brainstem slices were mounted with Mowiol® and coverslips were applied. For the 2 slices dedicated to non-specific staining, the primary antibody was omitted and substituted by an equal volume of PBS-NGS 1%.

4.2. Image acquisition and analysis

Immunolabeled tissues were examined under a Zeiss LSM 510 confocal microscope with a 20x magnification. Images were taken in the medial vestibular nucleus (MVN), with the border of the IVth ventricle as a landmark. For comparing NMDAR2 or AMPA staining between control and adapted mice, quantification of fluorescence was performed using ImageJ 1.50i software (NIH, USA). This was made through the drawing of a same size (220.23 x 214.26 µm) circle on each acquired image. Then, the mean value of fluorescence (level of grey) was calculated for one pixel for each MVN slice (NMDA, AMPA and non specific). The average of the two values for each staining (NMDAR2, AMPA and non-specific) was calculated for each mouse and the specific staining was calculated by subtracting the non-specific fluorescence to the desired receptor's fluorescence (NMDAR2 or AMPA).

5. GABAergic distribution in MVN of transgenic lines

In order to identify and further specify on which class of neurons the effects of VOR adaptation occur, future experiments will have to be conducted on transgenic lines. Since we observed specific effects of VOR adaptation on type A MVN neurons (see results, *In vitro* electrophysiological experiments) and as these neurons are largely GABAergic, we decided to explore their distribution in the MVN using different transgenic lines. We decided to visualize GABAergic neurons using the GAD67-GFP knock-in line, expressing GFP (green fluorescent protein) only in the neurons containing glutamic acid decarboxylase 67(GAD67). We also explored GABAergic neurons using two transgenic lines mainly used to observe interneurons in cortical layers: somatostatine-positive neurons (Sst-Cre) or parvalbumine-positive neurons (Pvalb-Cre), both expressing tdTomato only in these specific classes of GABAergic neurons.

To observe the distribution of these classes of neurons, the procedure used was repeated for the 3 transgenic lines. Mice were deeply anaesthetized by an intraperitoneal injection of pentobarbital (100 mg/kg) and injected with Heparine (50 mg/kg), to prevent blood coagulation. As soon as the anesthesia prevailed, they were intracardiacally perfused with phosphate-buffered saline (PBS, 0.1M) followed by 4% paraformaldehyde (PFA) fixative and the brains were carefully removed and placed in PFA for 24h and in sucrose solution (30%) for at least 48h. Like for the immunohistochemistry experiment, sections (80 µm) were cut in a freezing-slide microtome and were immediately placed in PBS 0.1M for 30 minutes. The wells were rinsed and 0.1mM DAPI was left to incubate for 20 minutes. After two washes of 10 minutes to remove the excess DAPI, the resulting brainstem slices were mounted in slides containing Mowiol® and coverslips were applied.

Slices were visualized using confocal microscopy (LSM 700, Carl Zeiss, Jena Germany) using the 10x and 20x objectives. The obtained images were adjusted for brightness and contrast and then stacked using ImageJ (Image processing and analysis in Java, USA).

6. Behavioral experiments

6.1. Video-oculography set-up

Video-oculography was performed to quantify how 2 weeks of visuo-vestibular mismatch affects the vestibulo-ocular reflex (VOR). Every mouse was placed at the center of a turntable at a ~30° nose-down position so that the horizontal canals were aligned in the yaw plane (Beraneck, et al. 2012). Throughout the experiment, the tested mouse stood restrained with a metal bar fixed to the headpost and with the body placed in a short Plexiglas tube. This restraint assembly was fixed on a rotating platform that stood on top of an extended rig with a servo-controlled motor. Images of the recordings are on **Annex 3**.

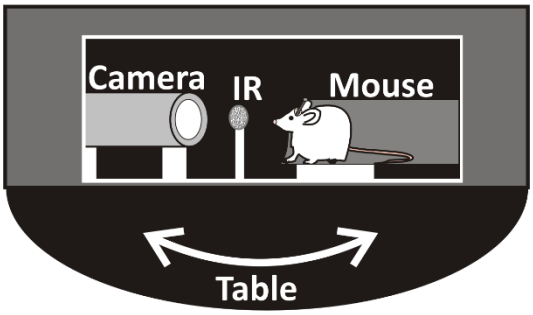

Figure 21. Illustration of the set-up used to test VOR. The mouse is head-fixed in a Plexiglas tube centered on a turn table. Eye movements are recorded by video-oculography performed in the dark. IR: Infrared light.

A miniature video camera, part of the video oculography system, tracks the eye movements during table rotations (**Figure 21**). By adjusting the Plexiglas tube with the camera in its central position, the recorded left eyeball could be translated left–right (X-axis) and the lenses could be focused. In addition, an infrared light beam pointed to the center of the pupil. The distance between the pupil and the corneal reflex was used to provide an accurate estimate of eye position.

Video-oculography measures were performed with all sources of light turned off except for the computer screen. The turntable is further surrounded with a closed black box to isolate the animal from remaining light, with a final intensity inside the box <0.02 lux.

6.2. Vestibulo-ocular reflex (VOR) recording sessions

Video-oculography was performed on two different groups of mice, wearing either striped or translucid device. This experiment was performed to record vestibulo-ocular reflex (VOR) performances. In total, 6 mice with the translucid device and 6 mice with the

striped device were tested. For each mouse, the VOR was tested prior to adaptation protocol. After the adaptation protocol (after 14 days with the device), the device was removed and VOR performances were also tested in this same day (day 0) and 1, 2, 6 days post adaptation.

Before starting the experiment, a drop of 2% pilocarpine (Laboratoire Chauvin, France) was applied in the mouse's left eye during 10 minutes in order to keep the size of the pupil constant. Horizontal VOR was tested using sinusoidal angular rotations around a vertical axis with different frequencies (0.2Hz; 0.5 Hz; 1 Hz; 2 Hz; fixed peak velocity 30°/s) and different velocities (20°/s; 30°/s; 40°/s; 50°/s; fixed frequency 0.5Hz).

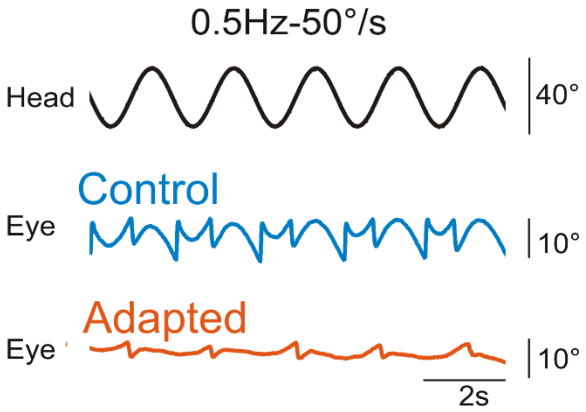

Figure 22. Example raw traces of the VOR in the dark recorded before (control, blue line) and after 2 weeks of visuo-vestibular mismatch (adapted, red line). In this example, the vestibular stimulation (head, black line) consisted in sinusoidal oscillation in the yaw plane at 0.5Hz and 30°/s. From Carcaud, França de Barros et al., 2016 under consideration.

6.3. Data acquisition and analysis

Eye movements were recorded using an infrared video system (ETL-200, ISCAN, Burlington MA). Eye and head position signals were sampled at 1 kHz, digitally recorded (CED power1401 MkII) with the Spike 2 software and later exported into the Matlab (The MathWorks) programming environment for off-line analysis. Analysis procedures were similar to those already reported (Beraneck et al. 2012). Horizontal eye and head movements data were digitally low pass-filtered (cut-off frequency: 40 Hz), and position data were differentiated to obtain velocity traces. Segments of data with saccades were excluded from analysis. At least 10 cycles were analyzed for each frequency. VOR gain and phase were determined by the least-squares optimization method. The variance accounted-for (VAF) of each fit was computed, and VAF values were typically between 0.70–1, where a VAF of 1 indicates a perfect fit to the data (Beraneck and Cullen 2007).

For each mouse, a gain and a phase value were measured for the different conditions (different frequencies with fixed velocity and different velocities with fixed frequency). As the experiment testing at different velocities with the same frequency gives similar results, the gain and phase values were averaged among the different velocities. This analysis allowed observing the effect of the visuo-vestibular mismatch protocol and studying the influence of the retinal slip on the VOR. For this purpose, only mice which have a VOR gain >0.5 were retained for further analysis (see Results, VOR adaptation protocols). After this selection, only 2 mice with striped device and no mice with translucid device were retained from my data set. For this reason, we combined my data to another set of data previously recorded in the team. In total, the effect of the tested frequency was observed on n=7 mice with the striped device and n=6 mice wearing the translucid device.

7. Statistical analyses

Statistical analyses were performed using Statistica 10 software (StatSoft, France). Repeated measures ANOVA (ANalysis Of Variance) as well as Post-hoc Tukey tests were performed on VOR gain measures depending on frequency or velocity. Non parametric unpaired Mann-Whitney tests were performed for comparing measures between control and adapted mice. The results were considered statistically significant when $p<0.05$. Results in the figures present mean ± SEM.

Results

The aim of this project was to study the neural changes underlying long-term VOR adaptation using in vitro whole cell patch clamp electrophysiology on brainstem slices. This part of the project was performed immediately after a two-week period of adaptation. Additionally, using video-oculography, I studied the role of the retinal slip error signal on the adaptation of the VOR. Finally, the test period was extended to 6 days after the removal of the device in order to explore the dynamic of the recovery (or re-adaptation period).

I. In vitro electrophysiological experiments

In order to study the neural changes that occur after the 14 days of VOR adaptation, I performed in vitro whole-cell patch clamp electrophysiology and recorded activity on brainstem slices of medial vestibular neurons from both adapted and control mice.

I. 1. Static properties of MVN neurons

I first studied the effect of VOR adaptation on static properties of MVN neurons. Primarily, and due to their pacemaker activity in brainstem slices, the characterization of the vestibular neurons responses was made without any external stimulation. The averages of the spike shapes and associated inter-spike intervals were used to obtain the parameters presented in **Table 3:** spontaneous firing rate (in spikes/s) and its coefficient of variation, the after-hyperpolarization potential (AHP, in mV), the double AHP (dAHP, in V/s), the after-hyperpolarization rectification (AHPR, in V/s), the spike threshold potential (in mV), the concavity and convexity of the inter-spike interval (in mV). The classification of the MVN neurons as type A or B was performed as described previously (see **Table 2**). Shown in **Table 3**, is also the statistical analysis (Mann-Whitney tests) of the difference between control and adapted mice in the three possible combinations (pooled control vs pooled adapted; control type A vs adapted type A; control type B vs adapted type B). Although most parameters do not reveal statistical significance, there is a significant difference between the firing rate (in Hz) of type A control and adapted neurons (firing rate of 12.77 vs 6.57, Mann-Whitney test, z z=1.96 p=0.049) and also between the amplitude of the after AHP between type B control and type B adapted neurons (AHP of 29.30 vs 27.60, Mann-Whitney test, z=-2.20, p=0.027). Overall, these results indicate that the electrophysiological signature of type A and type B neurons is mostly preserved by the adaptation. However, the decrease of type A neurons resting

discharge as well as the diminution of AHP of type neurons indicate that intrinsic membrane properties have been modified.

Table 3. Parameters of the resting spontaneous activity of MVN neurons recorded on control and adapted slices. Static parameters are based on the analysis of the spontaneous pacemaker discharge of the neurons and on the quantification of the after-hyperpolarization and interspike interval. Neurons are pooled (all) or segmented in type A and type B.

	All		Type A		Type B		Statistical tests (Mann-Whitney tests)		
	Control	Adapted	**Control**	Adapted	**Control**	Adapted	**Control** vs Adapted		
Number of neurons	38	24	23	7	15	17	All	Type A	Type B
Membrane potential (mV)	-47.58	-50.06	-47.68	-48.75	-47.30	-50.63	z=0.00 p=NS	z= 0.38 p=NS	z= 1.19 p=NS
Spike threshold (mV)	-30.25	-32.57	-30.36	-32.04	-30.58	-32.80	z= 1.59 p=NS	z=1.15 p=NS	z= 1.36 p=NS
Firing rate (Hz)	13.10	9.15	12.77	6.57	13.86	10.38	z= 1.88 p=NS	z=1.96 **p=0.049**	z= 1.42 p=NS
Coefficient of variation	0.16	0.22	0.18	0.29	0.13	0.24	z=-1.34 p=NS	z=- 1.45 p=NS	z=-0.62 p=NS
AHPR (V/s)	0.28	0.16	0.48	0.38	0.02	0.07	z= 0.93 p=NS	z=0.28 p=NS	z=- 0.73 p=NS
dAHP (V/s)	0.53	0.94	0.00	0.00	1.11	1.35	z= -1.23 p=NS	NA NA	z=-0.71 p=NS
AHP (mV)	26.96	27.33	28.63	27.60	29.30	27.60	z= -0.65 p=NS	z=-0.28 p=NS	z=-2.20 **p=0.027**
Concavity (mV)	-1.53	-2.20	-2.31	-4.74	-0.49	-1.09	z= -6.64 p=0	z=1.71 p=NS	z=1.21 p=NS
Convexity (mV)	0.70	0.74	0.50	0.15	0.88	0.95	z= 0.11 p=NS	z=1.61 p=NS	Z=0.02 p=NS

I. 2. Dynamic properties of MVN neurons

Then the active membrane properties of MVN neurons were examined by the injection of step-like stimulations.

2.1. Current-frequency curves

First, I performed current-clamp recordings and used step-like currents to ultimately allow the construction of current-frequency curves (I/F curves).

Figure 23 shows that the current injected has a notorious effect in all control and adapted neurons; when the current is increased, the frequency of discharge of the neurons also increases (adapted: ANOVA repeated measures, *group* effect, $F_{1,44}$=93,52, p=0.00; control: ANOVA repeated measures, *group* effect, $F_{1,68}$=182,12, p=0.00).

When pooled together, control and adapted neurons show no significant differences between their frequencies of discharge (ANOVA repeated measures, *group* effect, $F_{1,52}$=0,93, p=NS) (**Figure 23**A).

On the other hand, when the segmentation between type A and type B neurons is performed, differences between these two types of neurons arise. Adapted type A neurons (**Figure 23**B) show a decrease in the frequency of discharge in comparison to control type A neurons (ANOVA repeated measures, *group effect,* $F_{1,26}$=7,58, p<0.05). By contrast, adapted type B neurons (**Figure 23**C) show a current-frequency curve similar to that of control type B neurons (ANOVA repeated measures, *group* effect, $F_{1,24}$=0, p= NS).

This experiment revealed that the long-term adaptation protocol induced a decrease of excitability on a specific subpopulation of MVN neurons, the type A neurons, whereas it had no effect on type B neurons. This result clearly demonstrated an effect of VOR adaptation on dynamic properties of MVN neurons.

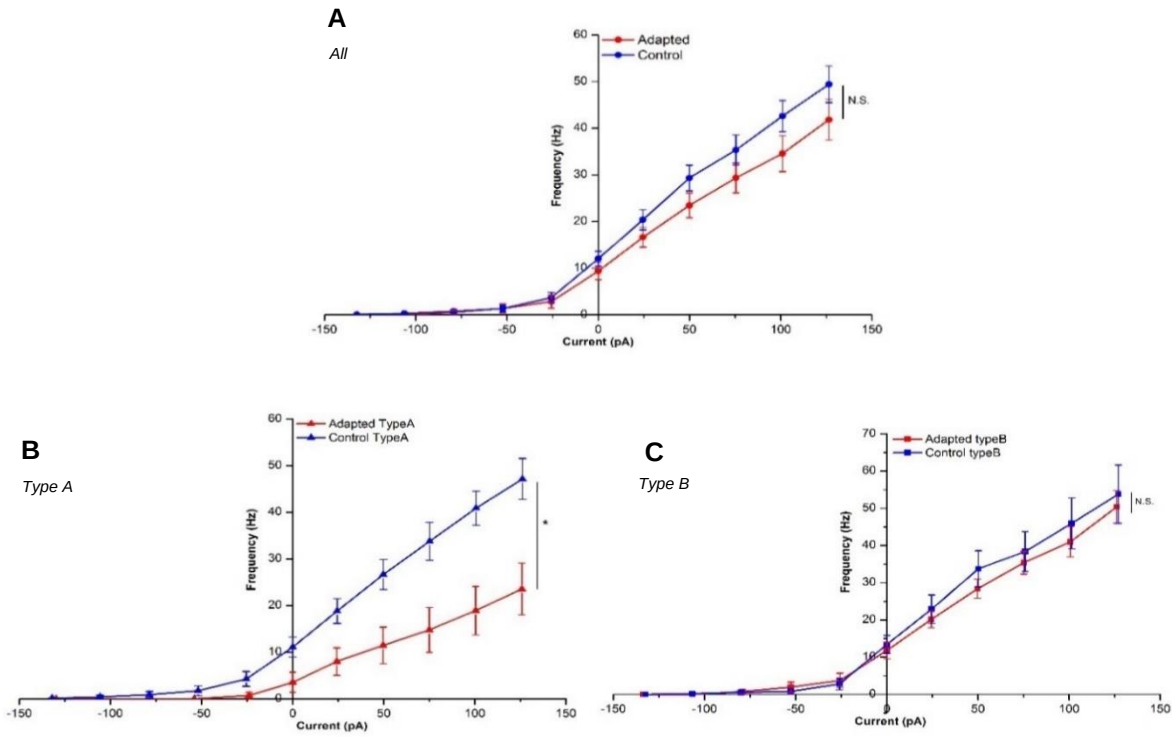

Figure 23. (A) Mean current-frequency relationship between control (n=38, blue line) and adapted (n=24, red line) neurons pooled together. (B) Mean current-frequency relationship between type A control (n=23, blue line) and adapted neurons (n=7, red line) and (C) between type B control (n=15, blue line) and adapted neurons (n=17, red line). Error bars represent ± SEM.

2.2. Current-voltage curves

I then analyzed active membrane properties by the injection of hyperpolarizing and depolarizing step-like currents, clamped at different voltages, which allowed to create current-voltage relationships.

These 3 curves (I/V curves) were constructed by plotting the mean amplitude for each clamped potential: -70± 20mV; 40±20 mV; -10±20 mV. For graphical purposes, the x axis crosses the y axis at the potential clamp in each experiment. Statistical analyses were only performed for the clamped potential of -70mV, the sole case in which the sample size is big enough to ensure the validity of the statistical tests.

At a hyperpolarized membrane potential of -70mV, no significant differences were found in the response to the injected current between the control and adapted groups (ANOVA repeated measures, *group effect*, $F_{1,53}$=0.09, p=NS) (**Figure 24**A). Even after the segmentation of MVN neurons in type A and type B, no significant differences were found between these I/V curves (type A: ANOVA repeated measures, *group effect*, $F_{1,30}$= 0.01, p=NS; **Figure 24**B) (type B: ANOVA repeated measures, *group effect*, $F_{1,21}$= 2, p=NS; **Figure 24**C).

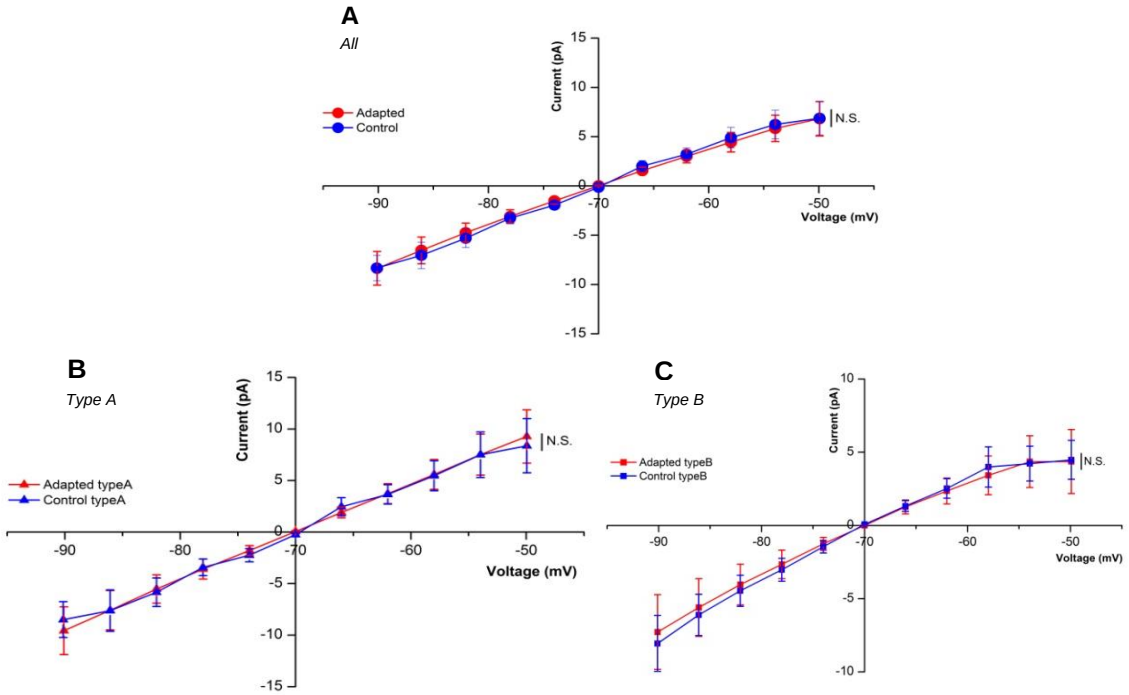

Figure 24. (A) Mean current-voltage relationship between control (n=40, blue line) and adapted (n=24, red line) neurons. Potential clamped at -70 mV. (B) Mean current-frequency relationship between type A control (n=25, blue line) and adapted neurons (n=8, red line). (C) Mean current-frequency relationship between type B control (n=15, blue line) and adapted neurons (n=16, red line). Error bars represent ± SEM.

At a clamp potential of -40mV (**Figure 25**A) the control and adapted neurons show no major differences between the sensitivity to the injected currents, although a slight divergence in the curves is noticeable at higher voltages. It seems that type A adapted neurons show a decreased slope, i.e. decreased currents for the same potentials, in comparison to type A control neurons (**Figure 25**B). Nevertheless, this effect is doubtable by the fact that only 3 type A adapted neurons were recorded in this experiment. For type B neurons, there is also a strong difference at lower currents (-20 pA to 0 pA) between adapted and control neurons. This difference can also be questionable since the number of recorded adapted neurons is not big enough, confirmed by the clear associated big error bars (**Figure 25**C). Thus, these results will need to be confirmed in future experiments.

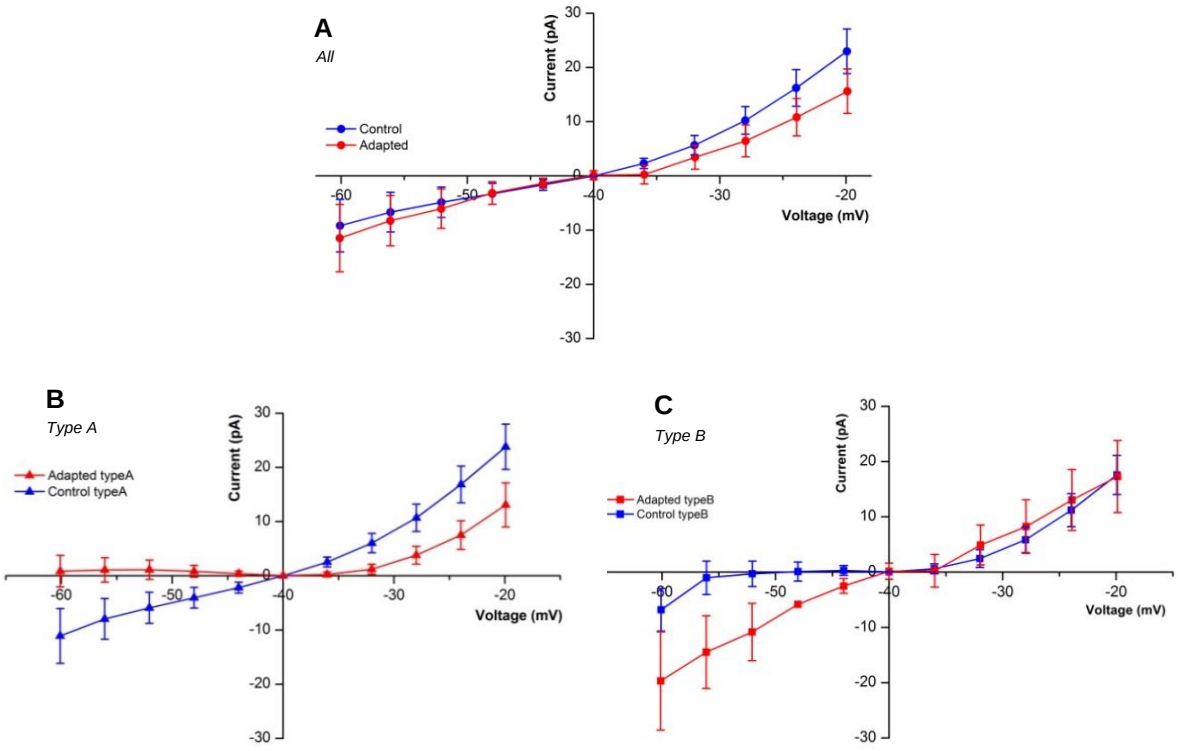

Figure 25. (A) Mean current-voltage relationship between control (n=28, blue line) and adapted (n=12, red line) neurons. Potential clamped at -40 mV. (B) Mean current-frequency relation between type A control (n=15, blue line) and adapted (n=3, red line) neurons. (C) Mean current-frequency relationship between type B control (n=13, blue line) and adapted (n=9, red line) neurons. Error bars represent ± SEM

At a clamped potential of -10mV, the control and adapted neurons pooled together show no significant differences (**Figure 26**A). Both adapted type A (**Figure 26**B) and type B (**Figure 26**C) seem to differ from their control counterparts, but again these differences cannot be conferred due to the rather low number of neurons recorded for both cases (3 and 9 respectively).

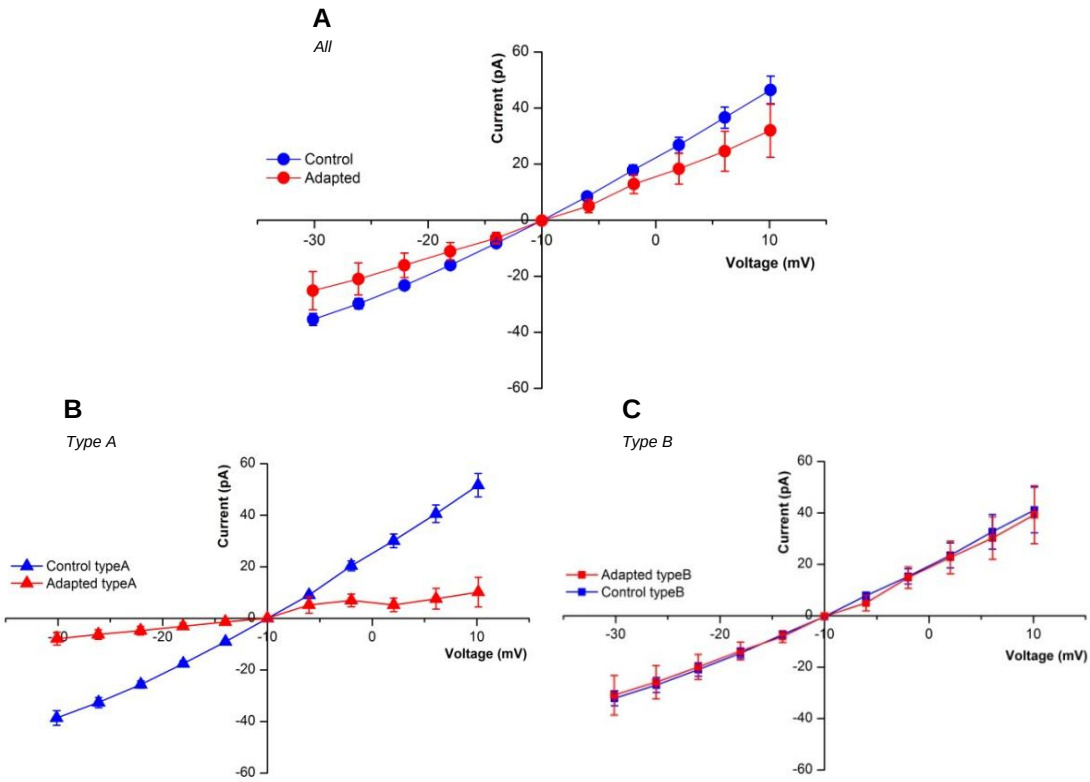

Figure 26. (A) Mean current-voltage relationship between control (n=14, blue line) and adapted (n=9, red line) neurons. Potential clamped at -10 mV. (B) Mean current-frequency relation between type A control (n=9, blue line) and adapted A (n=2, red line) neurons. (C) Mean current-frequency relation between type B control (n=7, blue line) and adapted B (n=7, red line) neurons. Error bars represent ± SEM.

I. 3. Synaptic plasticity after VOR long-term adaptation

After exploring the static and dynamic intrinsic properties of MVN neurons, the effect of VOR adaptation on the synaptic properties was then investigated.

The efficiency of the synapse between the vestibular afferent and MVN neurons was evaluated by recording excitatory post-synaptic currents (EPSCs), evoked through the stimulation of the VIIIth (vestibulocochlear) nerve. The amplitude (pA), area under the curve (AUC, fC) and time constant (tau, ms) of the evoked EPSCs were calculated in control and adapted conditions.

The AUC of an EPSC measures represents the quantity of charge transfer at the level of the synapse. As shown in **Figure 27**A, the AUC is smaller after long-term VOR adaptation compared to control (Mann-Whitney test, z= -2.85, p<0.01), showing that the synapse efficiency is decreased in the adapted condition. This decrease could reflect a change in the presynaptic release of neurotransmitter or a change in the postsynaptic receptor subunits.

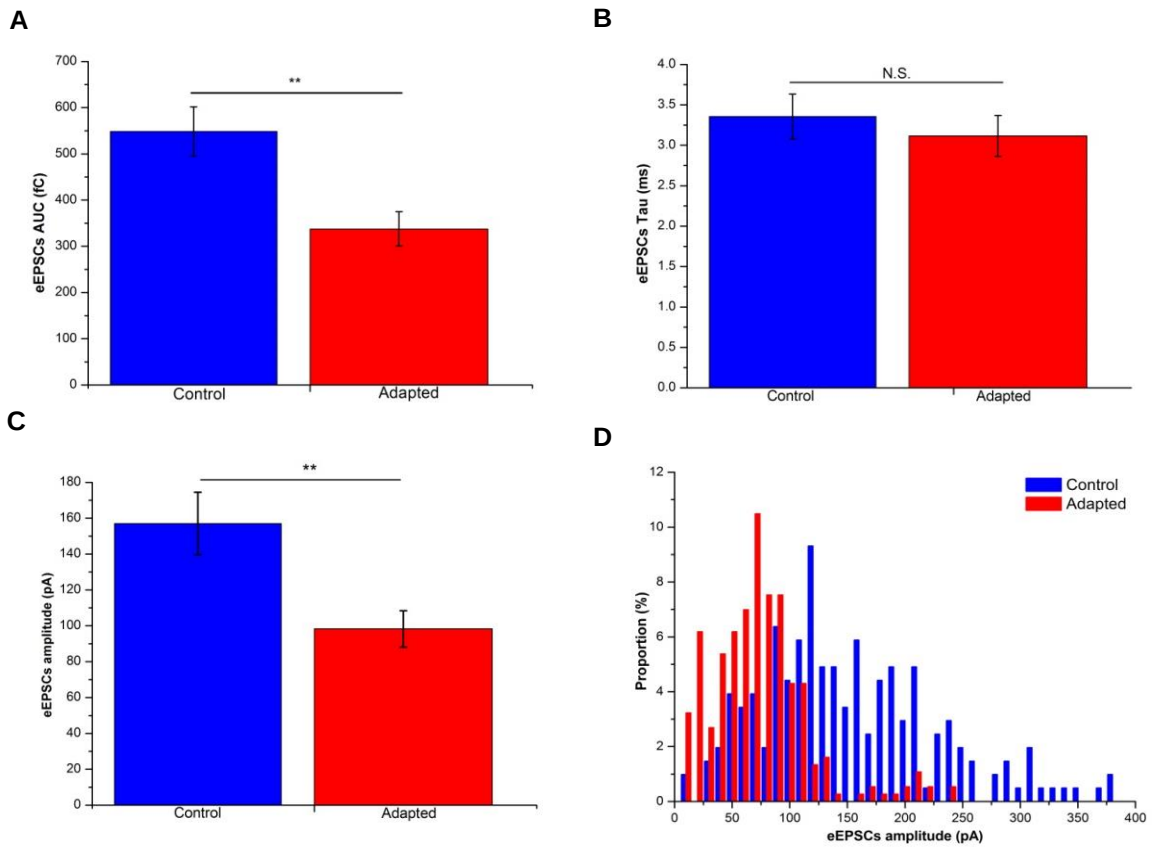

Figure 27. A) Evoked EPSCs area under de curve (AUC in fC) on control (n=17, blue bar) and adapted mice (n=31, red bard), (B) time constant (tau in ms) and (C) amplitude (in pA) recorded from control neurons (n=17, blue bars) and after VOR adaptation (n=31, red bar). Error bars represent ± SEM. (D) Distribution of EPSCs amplitude clearly showing that EPSCs after VOR adaptation have smaller amplitudes than on control.

To determine if this decrease in eEPSCs AUC depends on changes in the composition of the postsynaptic receptors, I explored the kinetic characteristics of the EPSCs. The eEPSCs time constant (τau) is not different between the 2 groups (**Figure 27**B, Mann-Whitney test, z=-0.88, p=NS) while its amplitude is smaller following the long-term adaptation in comparison to control mice (**Figure 27**C Mann-Whitney test, z=-2.58, p<0.01). This result is also confirmed in **Figure 27**D, representing the distribution of the eEPSCs amplitude in both groups (control and adapted), showing that EPSCs in adapted mice display a smaller amplitude on average (~50-100pA) when compared to those of control mice (200-400pA). As the time constant is similar between the 2 groups, it suggests that the receptor units involved in the eEPSCs responses are qualitatively not different between adapted and control mice. Thus, the observed change could reflect a change in the amount of postsynaptic receptors expressed at the membrane of MVN neurons.

Overall, this experiment demonstrates that the long-term VOR adaptation also depends on the reduction of the efficiency of the synapse between the vestibular

afferents and the second-order vestibular neurons, in addition to the plasticity on intrinsic properties of MVN neurons found previously.

II. Immunohistochemistry experiment

Several hypotheses could explain the observed synaptic plasticity within the vestibular nucleus: i) a change in the quantity of the neurotransmitters release; ii) a change in the quantity of receptors expressed; iii) a change in the affinity between the neurotransmitters and the receptors.

Hence, the decrease of the EPSCs amplitude in adapted mice (seen in **Figure 27**) could be related to a decrease of the expression of the receptors involved in synaptic transmission between the VIIIth nerve and the vestibular neurons. In order to this hypothesis we performed immunohistochemistry analysis on two of the receptors known to mediate the main vestibular inputs: NMDA and AMPA (Sans et al., 2000). The experiments were performed for both receptors on control and adapted mice.

Figure 28 shows the receptor-specific staining results for both control and adapted conditions for NMDA receptors (NR2 subunit), AMPA receptors (subunit GluR2 and GluR3) and for non-specific staining (negative control). Images of the Purkinje cells were taken in order to confirm that the staining was successful (positive control).

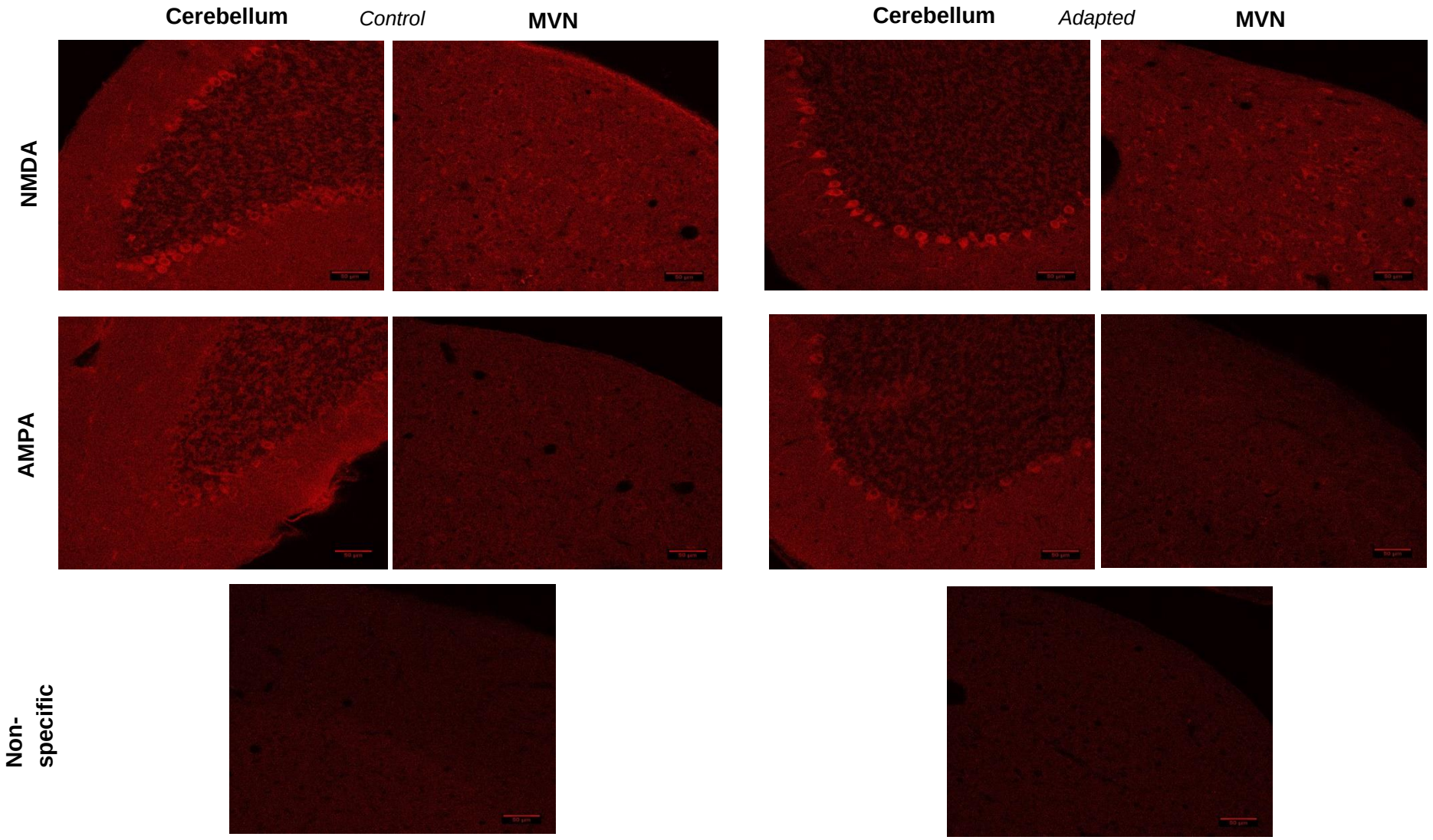

Figure 28. Immunohistochemical detection of the NMDA and AMPA receptors in the MVN of control (left panel) and adapted (right panel) mice. Positive controls are showed with images of the cerebellum Purkinje cells in the cerebellum. Scale bars: 50μm.

Although both receptors were detected in the MVN, NMDA (Mann-Whitney test, z=0.24, p=NS) and AMPA (Mann-Whitney test, z=0.24, p=NS) staining results show no significant differences between control (n=9) and adapted (n=8) conditions (**Figure 29**). This result suggests that the decrease of synaptic efficiency cannot be linked to a decrease of a specific subtype of glutamatergic receptor.

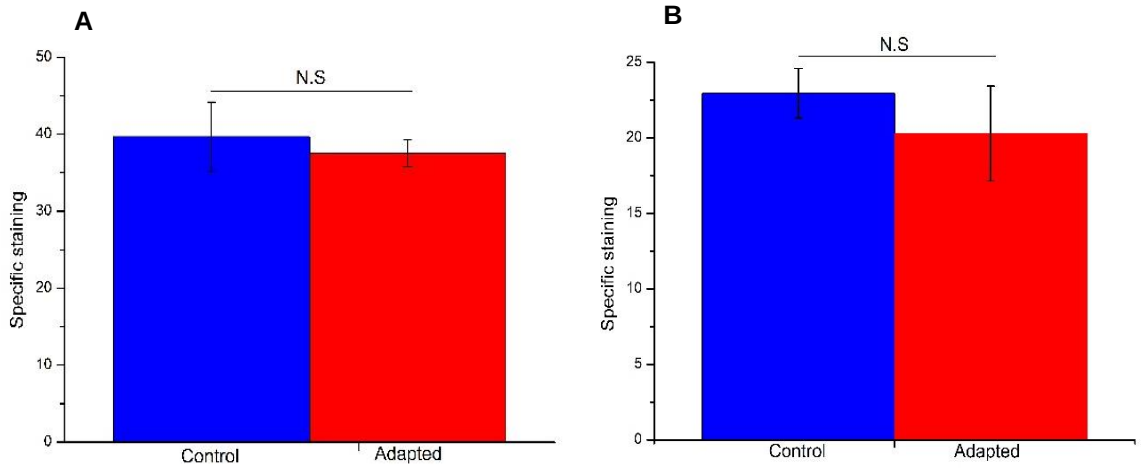

Figure 29. Mean specific staining for NMDA (NR2) (A) and AMPA (GluR2 and GluR3) (B) expression in the MVN in control (blue bars) and adapted conditions (red bars). Error bars represent ± SEM

Overall, the results presented so far extend and complete a comprehensive study, which demonstrates that long term VOR adaptation depends on changes within the brainstem, at the level of the MVN neurons. These changes involve both a change in the synaptic properties that links vestibular afferents to central vestibular neurons and changes in the intrinsic properties of vestibular neurons, and more specifically the subpopulation of type A neurons.

Given these results, I conducted additional exploratory experiments which set the basis of future studies: first, I explored the use of genetically-engineered mice strains to allow future specific recordings of type A neurons. Second, I performed behavioral experiments to determine the role of the retinal slip in the VOR adaptation and extended the tests to the first week following removal of the visuo-vestibular mismatch.

III. Identification of neurons

As presented in **Figure 23**B, long-term adaptation decreases the frequency of discharge of type A neurons when compared to their control counterparts. Because Type A neurons are in large part GABAergic (Rossert and Straka, 2011, Eugene et al., 2007, Eugene et al., 2011). we decided to observe the presence and the innervations of this subpopulation of neurons by using three different lines of genetically-engineered mice with fluorescent GABAergic neurons: GFP (GAD67), tdTomato Sst-Cre and Pvalb-Cre fluorescent proteins.

Using the GAD67 mice, this experiment allowed to visualize the anatomic distribution of all the GABAergic neurons present on the MVN. As expected, the GAD67-GFP (**Figure 30**A) neurons showed a wide spread distribution across the MVN.

GABA neurons expressing somatostatin (Sst) were also present in the MVN. The somatostatine-positive neurons (**Figure 30**B) are present in fewer quantities but in an even fashion throughout the MVN even though the number of neurons present is inferior in comparison to GABAergic neurons stained in the GAD67 line.

Parvalbumine-positive neurons distribute heterogeneously across the MVN, with a more peripheral expression, as it can be seen on **Figure 30**C. A scheme of the region of the brainstem (specifically, medial vestibular nucleus) where the images were taken is shown in **Figure 30**D.

This experiment shows the heterogeneous expression in the MVN of the different GABAergic neurons. It also encourages further experiments that will target a specific subset of vestibular neurons.

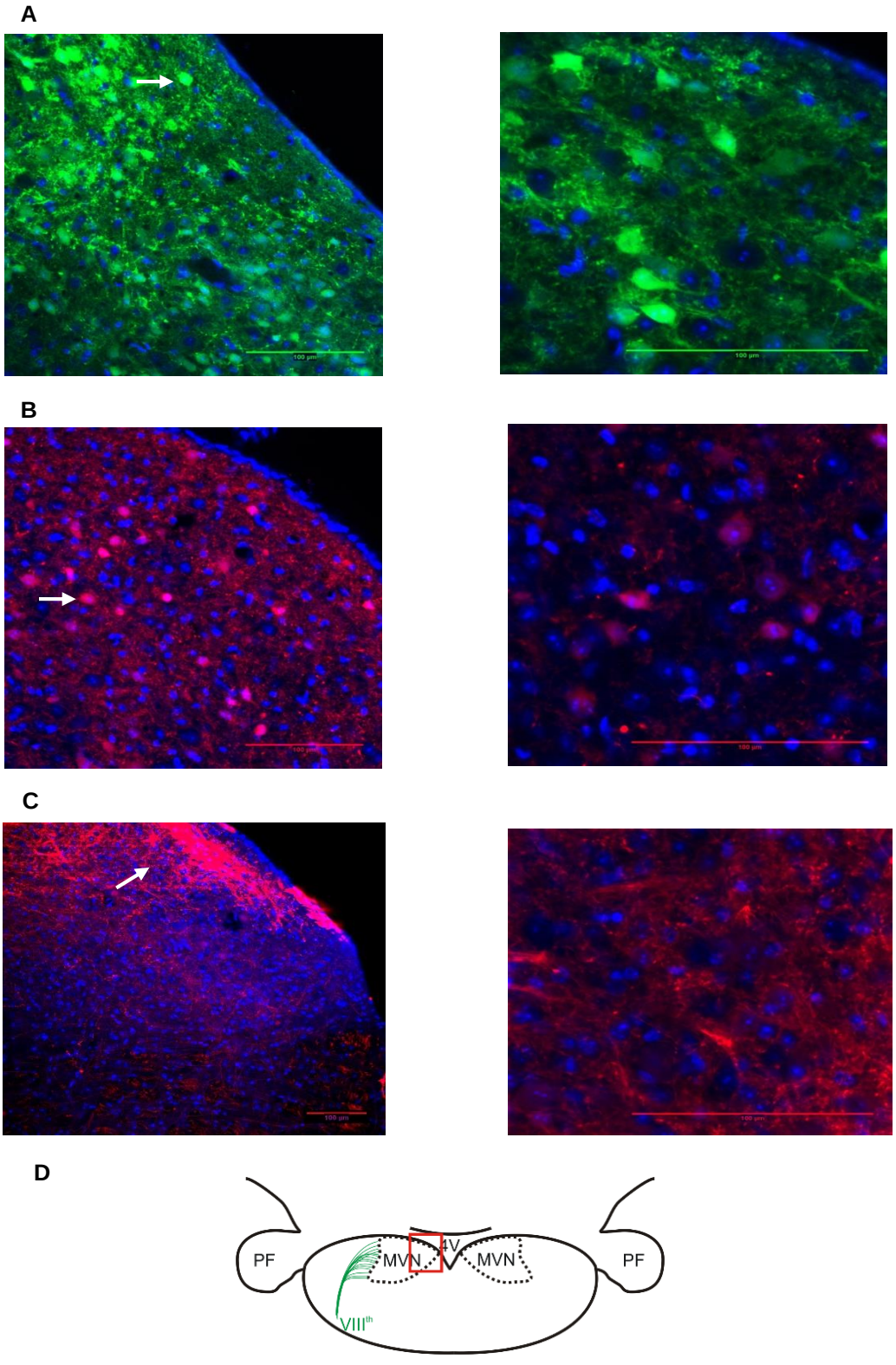

Figure 30. Confocal microscopy images of 80 µm coronal brainstem slices of transgenic mouse lines (20x and 40x). White arrows indicate the neuron targeted in each line. (A) GAD67-GFP positive neurons; (B) somatostaine-postive neurons (Sst-Cre); (C) parvalbumine positive neurons (Pvalb-Cre). Scale bars represent 100 µm. (D) Associated schematic representation of the location of the images in the brainstem.

IV. VOR adaptation protocols

The protocol used during my master thesis is a new paradigm which has never been used in rodents. It therefore raises many experimental questions, some of which are addressed in the following experiments.

IV. 1. The learning persists for several days

The first question is whether this long term adaptation engraved within the brainstem persists after the removal of the device, i.e how rapid is the unlearning (or the readaptation)? To investigate this point, VOR was tested before and several days (0; 1; 2; 6 days) after the end of the 14 day of visual vestibular mismatch (VVM). The data presented in the next figure follow the selection criteria mentioned in the Materials and Methods.

Analyzing the VOR responses under the same conditions at several time points allows to answer this question. Horizontal VOR in dark was recorded before and after VVM, at a fixed frequency of 0,5 Hz and with several velocities (20°/s-50°/s). Since the VOR gain was always similar between the different velocities tested, the performances at different velocities were averaged for all the mice tested and plotted against time. **Figure** represents the mean VOR gain normalized to the “before” (day prior to the VVM) value for the mice adapted to the striped device. The gain values for the mean of the velocities tested are statistically different during the different days measured (ANOVA repeated measures, *time effect*, $F_{4,24}$=13,62, p<0.001). After the two weeks of VVM (day 0), there is a significant decrease of approximately 70% of the VOR gain. This notable decrease between “before” and “day 0” confirms that the striped device induces a marked VOR adaptation (before vs day 0, Tukey HSD, p<0.001). In addition, the VOR gain remains very low and doesn’t go back to the initial value during the 6 following days (before vs day1, before vs day2, before vs day6: Tukey HSD, p<0.001). After a week of readaptation the gain appears to be still decreased by about 50% of its initial value, not changing significantly since day 0 until the end of the experiment (day 0 vs day 6, Tukey HSD, p=NS). This indicates that the adaptation persisted and that the learning signal has been engraved in the oculomotor circuitry. Thus, validating the notion of “long term”, very persistent, memory used throughout my master thesis.

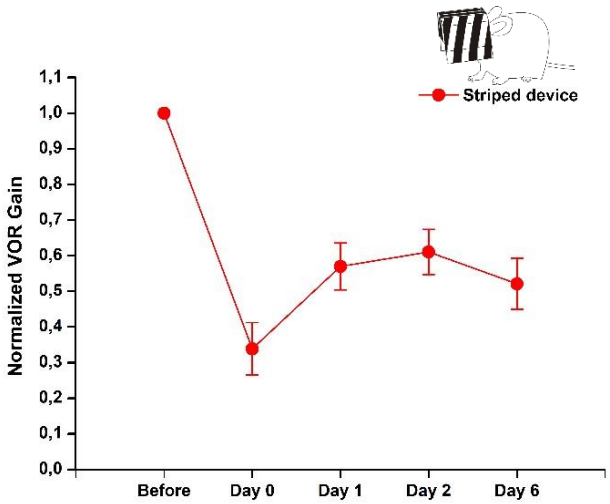

Figure 31. Mean VOR gains plotted in function of time (days) (each point represents the average of the tested velocities: 20°/s; 30°/s; 40°/s; 50°/s; fixed frequency of 0,5 Hz) for the striped device (red line, n=7). For each temporal scale presented from now on, the "Before" day represents the day prior to the adaptation and "Day 0" the day in which the device is removed from the mouse. Hence, between "before" and "day0" there is a difference of 14 days. Error bars represent ± SEM.

To thoroughly examine the individual variability between each mouse in response to the adaptation, I plotted the mean VOR responses per each mouse trough time (**Figure 32**). This graph confirms the response found in **Figure 31**; every mouse shows that the adaptation occurred at day 0 and its subsequent persistence along the next six days. This figure emphasizes that, despite a strong inter individual variability, the vast majority of the animals do not recover a pre-adaptation gain in 6 days of unlearning.

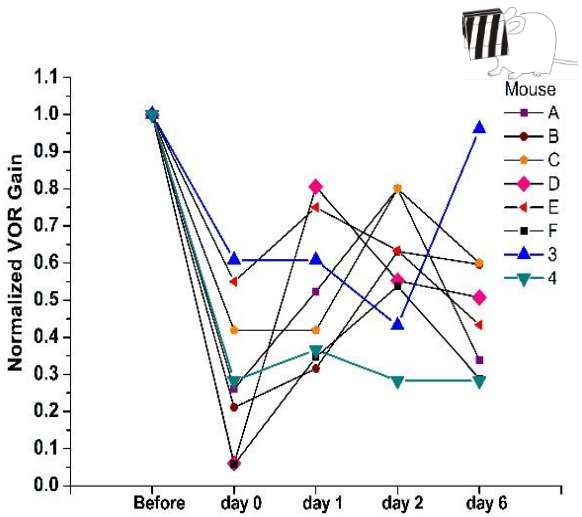

Figure 32. Normalized mean of VOR gains (tested velocities: 20º/s, 30º/s, 40º/s and 50º/s; fixed frequency of 0,5Hz) plotted in function of time (in days) for each mice using the striped device (n=7).

IV. 2. Effect of the tested frequency on the VOR

In the previous shown experiments, the persistency of the learning was observed at a particular frequency of 0.5Hz. Therefore, I next questioned whether the observed VOR adaptation happens at all frequencies. For that purpose, VOR was recorded in dark with a fixed velocity of 30 º/s with different frequencies ranging from 0.2 to 2 Hz (**Figure 33**).

VOR adaptation was induced for the whole range of the frequencies tested. This is demonstrated by the fact that the gain values were statistically different for the different frequencies tested (ANOVA, repeated measures, *frequency effect*, $F_{3,21}$=73,47, p=0.00). Remarkably, between 0.2Hz and every tested frequency as well as between 2 Hz and every tested frequency, the gain values are always statistically different for the days tested (0.2 Hz vs 0.5 Hz, 0.2Hz vs 1 Hz, 0.2 Hz vs 2Hz: Tukey HSD, p<0.01). On the other hand, at all the days tested, the gain values were statistically not different between 0.5Hz and 1 Hz (Tukey HSD test, p=N.S); despite not existing a statistical difference at 1Hz the recovery is faster than as 0.5Hz.

The gain values were also statistically different for the different days tested (ANOVA repeated measures*, time effect*, $F_{4,28}$=26,60, p=0.00). This means that the adaptation persists during all the days and for every tested frequency. At all the frequencies tested, the gain values were only statistically not different between day 1 and day 2 (Tukey HSD test, p=N.S), day 1 and day 6 (Tukey HSD test, p=N.S) and day 2 and day 6 (Tukey HSD test, p=N.S). This means that, from day 1 until day 6, the gain values stay more or less the same. For every frequency tested there is also a notorious decrease in the gain between before and after the VVM protocol (before vs day 0, Tukey HSD test, p<0.001), demonstrating that VOR adaptation was induced for the range of frequencies tested. Additionally, between before and every tested day, the VOR gain values were always statically significant (before vs day 1, before vs day 2, before vs day 6: Tukey HSD test, p<0.001), meaning that the VOR gains recoveries did never fully occur.

Nonetheless, it is possible to observe that the adaptation endured longer for the lowest frequencies (0.2 Hz and 0.5Hz) compared to the highest frequencies (1 Hz and 2 Hz) since the VOR gains values stay further away from its corresponding before value. Hence, it is possible to say that VOR adaptation is frequency-dependent and its recovery is more efficient at higher frequencies. This result illustrates the frequency-dependent differential role of the visual inputs (and of the optokinetic system) in the tuning of the vestibular system. It also shows that adaptation is most efficient and persistent at the

frequency where most of the natural head movements of the mouse occur (Beraneck et al. 2008).

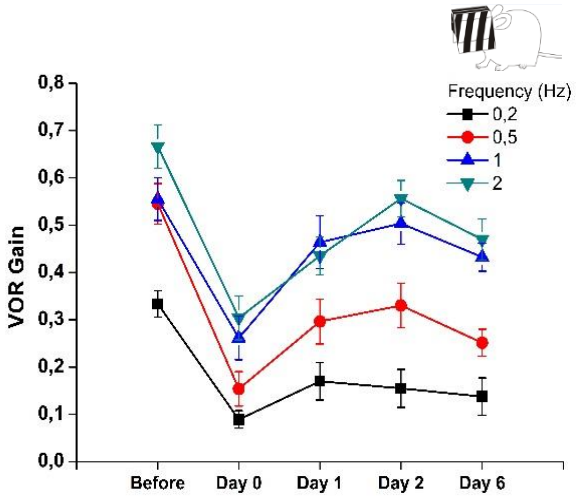

Figure 33. Mean VOR gain, in function of time (days), per each tested frequency at a fixed velocity of 30°/s. Black line: 0.2 Hz; red line: 0.5 Hz; blue line: 1 Hz; green line: 2 Hz. Striped condition. Error bars represent ± SEM.

IV. 3. The retinal slip drives motor learning

To determine if the retinal slip drives the motor learning, as it is hypothesized in the literature, I compared the VOR responses of the striped and translucid devices (see Materials and Methods). Therefore, I performed the same experiments referred above in mice adapted with a translucid device that provides a less contrasted visual surround.

Horizontal VOR in dark was recorded before and after VVM, at a fixed frequency of 0,5 Hz and with different velocities (20°/s-50°/s). Since the VOR gain was always similar between the different velocities tested, the performances at different velocities were averaged for all the mice tested and plotted against time. **Figure 34** represents the mean VOR gain normalized to the "before" (day prior to the VVM) value for the mice adapted to the striped device. The gain values for the mean of the velocities tested are statistically different during the different days measured (ANOVA repeated measures, *time effect*, $F_{2,10}$=11,60, p<0.01) Interestingly, the decrease in VOR gain from "before" to "day 0" was the same reported for the striped device (approximately 70%) (before vs day 0, Tukey HSD, p<0.01). This suggests that the marked decrease seen for both conditions can either depend on the retinal slip or on a decalibration of the VOR. Contrarily, in the translucid condition, 2 days after VVM removal the VOR gain mostly returns to its initial value (before vs day 2, Tukey HSD, p=NS). This rapid unlearning suggests that the strength of the learning does depend on a strong retinal slip.

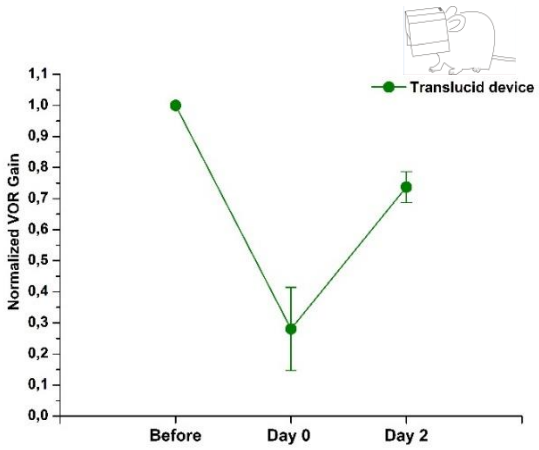

Figure 34. Mean VOR gains plotted in function of time (days) (each point represents the average of the tested velocities: 20°/s; 30°/s; 40°/s; 50°/s; fixed frequency of 0,5 Hz) for the translucid device (green line, n=6). For each temporal scale presented from now on, the "Before" day represents the day prior to the adaptation and "Day 0" the day in which the device is removed from the mouse. Hence, between "before" and "day0" there is a difference of 14 days. Error bars represent ± SEM.

To confirm each mice's response to the adaptation, I plotted the mean VOR responses per each mouse trough time (**Figure 35**). Although mouse E and F do not follow the trend, **Figure 35** shows that the adaptation occurred at day 0 and that there was less persistency than with the stripped helmet along the next two days.

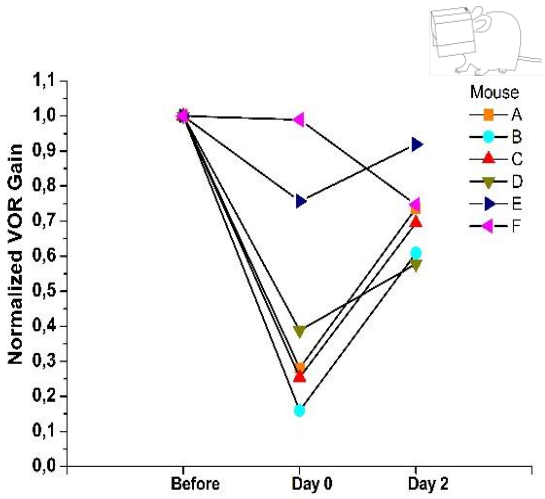

Figure 35. Normalized mean of VOR gains (tested velocities: 20º/s, 30º/s, 40º/s and 50º/s; fixed frequency of 0,5Hz) plotted in function of time (in days) for each mice (n=6). Translucid condition.

Following, I studied at which frequencies the VOR decrease happens. For that purpose, VOR was recorded in dark with a fixed velocity of 30 º/s with different frequencies ranging from 0.2 to 2 Hz.

VOR adaptation with the translucid device was also induced for the whole range of the frequencies tested (ANOVA repeated measures, *frequency* effect, $F_{3,15}$=22,45, p<0.001). Similarly to the striped condition, at the lowest frequencies the VOR gains have the lowest values throughout the duration of the protocol, with statistical significance when compared to the highest frequencies (frequency 0.2Hz vs 1Hz, 0.2 Hz vs 2Hz, 0.5 Hz vs 1Hz, 0.5Hz vs 2Hz: Tukey HSD test, p<0.001). On the other hand, no differences were found between the highest frequencies (1Hz vs 2Hz Tukey HSD test, p=N.S).

The gain values were also statistically different for the different days tested (ANOVA repeated measures, *time effect*, $F_{2,10}$=18,62, p<0.001). For every frequency tested there is also a notorious decrease in the gain between before and after the VVM protocol (before vs day 0, Tukey HSD test, p<0.01), demonstrating that VOR adaptation was induced for the range of frequencies tested. Nevertheless, for all the frequencies tested, there were no statistical differences between before and day 2 (before vs day 2, Tukey HSD test, p=N.S), meaning that the gain returned to its initial values revealing a weak and, therefore, short VOR adaptation (**Figure 36**).

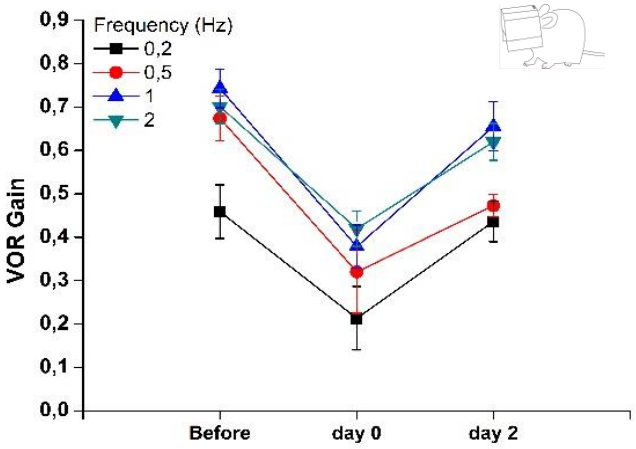

Figure 36. Mean VOR gain, in function of time (days), per each tested frequency at a fixed velocity of 30°/s. Black line: 0.2 Hz; red line: 0.5 Hz; blue line: 1 Hz; green line: 2 Hz. Translucid condition. Error bars represent ± SEM

Overall, these results demonstrate three main points. First, that the adaptation persists for several days after the removal of the device, which confirms that long-term adaptation process, is at stake. Second, that adaptation is most persistent at frequencies below 0.5HZ. Third, and final, that adaptation depends on a strong retinal slip, which drives the motor learning. At day 0 however, the VOR decreases are multi causal as they can be interpreted as a combination of both a reduction of the VOR (specific learning, frequency dependent) and as a decalibration of the VOR (unspecific and frequency independent).

Discussion

During the course of this project, a novel protocol to study long-term VOR adaptation was used. The cellular and molecular alterations that occur after VOR long-term adaptation were studied through the comparison between control and adapted mice. We obtained first direct evidence that long-term VOR adaptive memory is consolidated within the vestibular nuclei, especially at the synapse between the first and second-order vestibular neurons, accompanied with modifications of the excitability of a subpopulation of neurons (type A) in the medial vestibular nucleus (MVN). With the VOR adaptation protocol we demonstrated the persistency of the adaptation, especially at the lower frequencies, and confirmed the role of the retinal slip in driving the motor learning.

The advantages and limitations of the protocol we used to create the visuo-vestibular mismatch are hereby first discussed followed by the cellular and molecular hypothesis related to our findings.

1. VOR adaptation protocol

1.1. Advantages of the VVM protocol

VOR adaptation is commonly studied in humans and monkeys through the use of prisms that are worn by the subject for several days (Anzai, Kitazawa et al. 2010). On the other hand, in rodents the VOR gain-down adaptation is usually induced by the use of a turntable in which the head-fixed mouse is rotated while its visual field is also rotated (Broussard and Kassardjian, 2004). Hence, a visuo-vestibular conflict is created making VOR counterproductive. The long term VOR adaptation is then reached through iteration of an 1h training session on numerous consecutive days, which makes it a methodology that dispends a lot of experimental time, adding to the fact that usually a lot of mice need to be trained and recorded (Raymond and Lisberger 1996, Boyden and Raymond 2003). Besides, head-fixed protocols restrain the mouse to pre-defined frequencies/velocities and to training sessions that go on just for a limited amount of time per day. In addition, the vestibular stimulation is not generated actively since they impose involuntary movements to the mouse, thus representing a “passive” learning which greatly influences the vestibular processing (Cullen, 2012). While most of the *in vivo* experiments are performed on monkey and cats, *in vitro* cellular and molecular work is conducted on rodents. Due to this duality, the possible mechanisms of cellular plasticity that take place

during VOR adaptation are still considered with skepticism (Goldberg and Oxford University Press., 2012).

The inspiration for the presented visuo-vestibular mismatch (VVM) protocol in this project came to resolve part of these experimental discrepancies. The methodology developed by my group surpasses the experimental restrictions mentioned in the above paragraph. It consists in a VVM induced by a helmet-like device on the mouse's head that enables a free behavior, as do the prisms in human and monkey. Consequently, in this innovative protocol, the uninterrupted 14-day process of adaptation causes VOR learning through the response to voluntary natural head movements.

As we will see in the following parts of the discussion, this new protocol makes it possible to perform in the same animal experiments at the behavioral and cellular/molecular level, opening a new era in the study of VOR motor learning.

1.2. VOR adaptation following VVM protocol

Before my thesis, my group was already using the VVM with stripped helmet. However, the protocol was applied on all mice without any additional criteria. The team had produced data demonstrating that, in average, 15 days of VVM produce a roughly 50% VOR gain diminution. As we have mentioned above, this experimental paradigm is closer from the in vivo models than from the rodent head-fixed models used so far. However, we also have validated that the induced VOR adaptation resembles to the one produced during head-fixed protocols in terms of gain reduction and phase adjustments. This is a crucial point as it suggests that the cellular/molecular mechanisms are, in part, comparable.

On the group of mice I worked with, I noticed that some had a rather low initial gain ("before adaptation"). As we wanted to study the adaptation, with a low initial gain, any occurring changes would not have been adequately noticed. Therefore, a new criteria of a minimum VOR gain before adaptation of 0.5 was established. Like that, the decrease in the gain after the 14 days of adaptation could have an ample magnitude in order to be duly noted. This criteria, selected in the striped condition only two mice and discard all the four mice adapted using the translucid device. Even though throughout the whole protocol all the mice had the same age (starting the protocol at 3 weeks and ending at 6 weeks), the difference in the gains recorded between them could be due to biological differences. For example, a visual deficit or even the onset of puberty, which usually is variable even among animals of the same inbred strain (Fox, 2007). This

crucial methodological point has been identified during my master thesis. Its consequence is that in future studies, it will be necessary to record VOR before to induce VVM and to keep for in vitro work only animals which have an already >0.5 VOR gain.

1.3. Effect of the retinal slip on the VOR adaptation and recovery

The use of the two different patterns on the device (striped or translucid) was done with the purpose to test the effect of the retinal slip in the VOR adaptation. The retinal slip is strong with the striped device but probably minimal or absent with the translucid device. The VOR recordings showed that, in order to have a strong VOR adaptation, the presence of a strong retinal slip is needed. Although, the 14 days of VVM protocol induce a gain-down adaptation of the VOR with or without retinal slip, there is a notorious difference on the recovery of the VOR gain. The striped device, after the six days of the removal of the device, doesn't recover while, the translucid device's gain returns to its initial value after two days. Therefore, at day 0 the VOR decreases are multifactorial as they can be faced as a combination of both a reduction of the VOR (specific learning, frequency dependent) and as a decalibration of the VOR (unspecific and frequency independent).

1.4. Effect of the tested frequency on the VOR adaptation

Using this VVM protocol, a clear VOR adaptation is also shown at all tested frequencies (0.2Hz, 0.5Hz, 1Hz and 2Hz). This decrease is analogous to the ones obtained in the mentioned traditional head-fixed protocols (Boyden et al. 2004, Kassardjian et al. 2005). But the VOR adaptation has different effects on the tested frequencies.

When the VOR is tested for low frequencies, for the striped condition, there is no recovery during the six days following the removal of the device. This can be related to the fact that, naturally, mouse's head movements are done at low frequencies and thus, should be the ones more greatly affected by the adaptation (Beraneck et al., 2008). Additionally, the optokinetic reflex (OKR), which complements the VOR to stabilize vision during low frequency movements (Faulstich et al., 2006, Goldberg and Oxford University Press., 2012), is most efficient at lowest frequencies. Since the VOR adaptation is visually-induced, it is understandable that the adaptation concerns the frequencies where the visual, and not the vestibular system, is most efficient.

Interestingly, previous studies have demonstrated that the spread of adaptation is frequency-selective: when adaptation is performed at low frequencies like 0.2Hz or 0.5Hz, the learning spreads to other frequencies. If the learning is performed at a higher

frequency (1 or 2Hz), it remains specific to that particular frequency (Boyden et al. 2004, Kassardjian et al. 2005). In the case of the VVM, we have demonstrated that adaptation occurs around frequencies of 0.2 to 0.5Hz, and supposedly spreads to higher frequencies. Nevertheless, its retention seems to be more consistent at these frequencies where the adaptation occurred.

The VOR recovery was found to occur faster at higher frequencies than at low frequencies. At high frequencies the translucid condition shows recovery at day 2 while, in the striped condition, the recovery comes close to completion at day 6. This shows that VOR long-term adaptation was not induced at 1Hz and 2Hz in the translucid condition, and less robust in the striped condition. This could be due to the fact that the response to higher frequencies is dominated by the vestibular inputs of the VOR. These inputs are known to be governed by AMPA/NMDA receptors (Sans et al., 2000), which were tested immunohistochemically and qualitatively showed no alterations. Therefore, further pharmacological and electrophysiological studies will be needed in order to quantify the NMDA and AMPA components of the responses.

Overall, these results indicate that VOR adaptation is frequency dependent and that the VVM paradigm is more efficient for the frequencies below 0.5Hz.

2. *In vitro* electrophysiological experiments

In vitro patch-clamp recordings were performed on MVN neurons of brainstem slices from adapted and control mice. These recordings allowed studying the alterations caused by the VOR learning protocol to the neurons' intrinsic and synaptic properties.

2.1. Plasticity of the synaptic properties

Changes in the synaptic properties of MVN neurons were early on postulated as a possible adaptive mechanism following VOR learning (3.1. Possible sites of motor learning). Recently, Mitchell and her team (Mitchell et al., 2016) have demonstrated *in vivo* that plasticity in the brainstem was presumably mediated by synaptic changes in the VOR pathway.

In our study, we have observed a consistent decrease in the EPSCs amplitude, which is the first demonstration of an *in vitro* modifications following VOR adaptation paradigm. The decrease of synaptic efficiency at the level of vestibular afferent synapse onto vestibular nuclei neurons is in direct line with theoretical evidence which have

postulated a long-term change at these synapses (Masuda and Amari 2008, Menzies et al. 2010, Yamazaki et al. 2015).

What are the mechanisms underlying this decrease? In these experiments, we observed a decrease in the evoked excitatory post-synaptic currents (eEPSCs) area under the curve, meaning that adapted MVN neurons have a decrease in the quantity of ions (cations) released through the membrane when compared to control ones. This decrease of synaptic efficiency in adapted neurons is further confirmed with the decrease in the EPSC amplitude. The decrease of the EPSCs amplitude could be explained by different hypothesis: either a decrease of the release of the neurotransmitter quantity, or a decrease of the affinity of the excitatory receptors or finally a decrease of the number of receptors.

The release of neurotransmitter quantity can be tested by analyzing the miniature EPSCs, which reflect the spontaneous release of neurotransmitter vesicles. Recently, my group has recorded and analyzed the miniature EPSCs from control and adapted mice: this specific analysis demonstrated no difference between the 2 conditions, which indicates that the presynaptic release of neurotransmitter is probably not affected by the VVM.

In order to test the hypothesis of a decrease of the number of receptors, immunohistochemistry experiments were performed in brainstem slices of control and adapted mice. Both NMDA and AMPA receptors were detected in the MVN but no significant differences were found in the quantity of these receptors between control and adapted conditions. Hence, this result suggests that the decrease of synaptic efficiency is not related to a decrease of a specific subtype of glutamatergic receptor. To fully affirm this, more experiments would have to be done in the remaining subunits of both receptors (GluR1 and GluR4 as well as NMDAR1).

2.2. Plasticity of the intrinsic properties

Changes in the intrinsic excitability of MVN neurons were also hypothesized as a possible adaptive mechanism following VOR learning (du Lac, 1996).

First, the static properties of MVN neurons were studied. No major modifications after VOR adaptation were found. In another model of post-lesional plasticity, the static properties of MVN neurons were extensively modified, that is the electrophysiological signatures of type A and type B neurons revealed in depth modifications of the conductances implicated in the pacemaker activity of the neurons (Beraneck et al., 2003,

Beraneck et al., 2004). This is not the case following VOR long term adaptation. However, a change of the spontaneous firing rate of type A neurons was found between control and adapted mice, as well as a slight modification of the amplitude of the AHP of type B neurons. These 2 results have no direct functional interpretation, but are evidence of on-going plastic changes that differentially affect both subpopulations of neurons.

I then studied the dynamic properties of MVN neurons and found a modification of sensitivity revealed by the I/F curves in type A neurons after adaptation, while type B neurons remained unaltered. At this point, we have no evidence suggesting which conductances have been modified. These could obviously be the Na^+ and K^+ conductances implicated in the generation of the action potential, however we found no differences in the spike *per se*. Another possibility would be a change in the calcium homeostasis of the neurons, for instance in the calcium-dependent K+ conductances, calcium conductances and calcium buffering proteins which have been shown to be regulators of central vestibular neurons excitability (Eugene et al., 2011).

This result was further confirmed by the I/V curve at the highest clamped potential (-10mV and even -40mV), showing that type A adapted neurons, in comparison to type A control neurons, have decreased currents for the same injected potentials, demonstrating a decreased excitability. Even though there is not enough data to ensure the reliability of this last result, the observed trend confirms the result found with the I/F curve. However, this effect was not observed at really hyperpolarized membrane potential of -70mV. One putative explanation is that the conductances implicated in the responses differ greatly between hyperpolarized versus depolarized states.

Overall, our results indicate that type A neurons are probably a key player in the adaptive process. Type A neurons are thought to be local GABAergic interneurons or GABAergic neurons implicated in the commissural system. They however constitute a heterogeneous population and it will be therefore important in the future to be able to further discriminate the neurons according to additional criteria (Kodama et al., 2012) as, for instance, using genetically-engineered mice lines.

2.3. Heterogeneous population of MVN neurons

As mentioned, we found a decrease in the average size of the EPSCs from the vestibular afferent to the second order neurons. Based on previous experiments (Lisberger and Pavelko, 1988), it is probable that this decrease is not found in every vestibular neuron.

Hence, vestibular neurons constitute a heterogeneous population according to their neurotransmitter content, inputs received and projection areas.

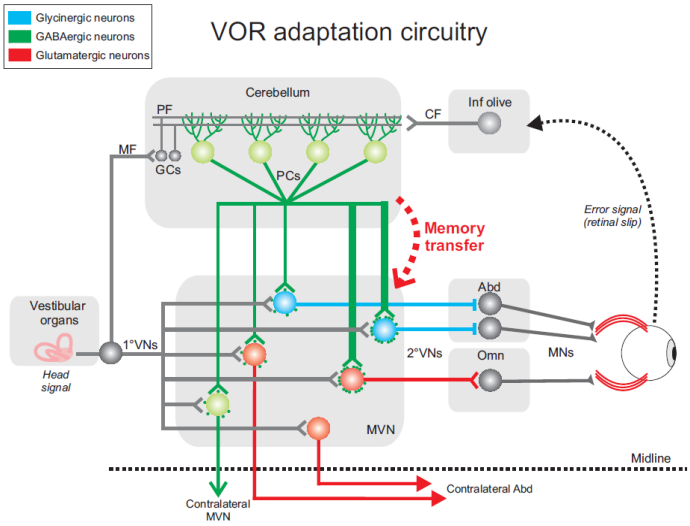

Figure 37. Circuitry of structures involved in VOR and its adaptation. First-order vestibular neurons (1°VNs) send head movement information to the medial vestibular nucleus (MVN). Subpopulations of second-order vestibular neurons (2°VNs) are partitioned depending on the density of innervations received from the flocculus and their neurotransmitter content. Densely or sparsely innervated glycinergic (blue) floccular target neurons (FTNs) project ipsilaterally to abducens nucleus (Abd), densely innervated glutamatergic FTNs (red) project ipsilaterally to oculomotor nucleus (Omn), sparsely innervated FTNs or non-FTNs glutamatergic neurons project contralaterally to abducens nucleus, and GABAergic FTNs (green) project to the contralateral MVN. Motoneurons (MNs) control the eye muscles contraction. During adaptation, the retinal slip error signal is sent to the inferior olive (Inf olive) and then to the cerebellum by climbing fibers (CF). Purkinje cells (PCs) integrate the error signal with vestibular information conveyed by mossy fibers (MF) and parallel fibers (PF) of granular cells (GCs), and in turn regulate the activity of 2° VNs. From Carcaud, França de Barros et al.,2016 (under consideration).

The above figure summarizes different group of vestibular neurons according to the input they receive from the flocculus; their neurotransmitter content and their projecting area. MVN neurons that receive cerebellar inputs are commonly called flocculus target neurons (FTNs). FTN integrate cerebellar and vestibular information and should have an instrumental role in the transfer of plasticity after long-term VOR adaptation (Broussard and Kassardjian, 2004). The role of Purkinje cells is to integrate the error signal with vestibular information and to regulate the activity of the vestibular neurons (Ramachandran and Lisberger, 2008).

On the long term, how could PCs affect FTNs? Our group results show that long-term VOR adaptation induces a decrease of the efficiency of the vestibular nerve synapses onto MVN neurons, probably trough long-term depression (LTD). So far, FTNs were not specifically targeted so the data reported is the mean reduction of the heterogeneous MVN population. It was previously shown that plasticity at this synapse can be induced by high frequency stimulation of vestibular afferents, and that the

direction of the plasticity is dependent on both the developmental stage (Puyal et al., 2003) and the stimulation pattern (Scarduzio et al., 2012) at resting potential. Moreover, previous studies found that this plasticity is also dependent on the postsynaptic membrane potential; short burst stimulation resulted in LTD if the neuron was at its resting potential or in LTP if the neuron was hyperpolarized (McElvain et al., 2010). These data suggest that PC inhibition could guide the strengthening of vestibular nerve synapses onto vestibular nucleus neurons. Therefore, the possible LTD reported could be explained by a mechanism of heterosynaptic plasticity. More experiments will be needed in order to decipher the mechanisms which underlie the transfer of memory from cerebellum to the brainstem.

Future perspectives

Following this master, many question arises which would deserve additional experiments. Some of which have already been presented in the discussion. I have listed below additional perspectives ranging from the behavior to the cellular and molecular level.

1. Different timescales

As can be seen, the VVM protocol performed is perfect to study any desired timescale (short or long). It is known from post-lesional studies that neuronal membrane properties modifications are qualitatively and quantitatively wider after a month of adaptation than after 10-15 days (Beraneck and Idoux 2012). Therefore, as future perspectives for the behavioral experiment, we intend to perform behavioral tests in which the time of the VVM protocol is extended from 14 to 30 days. This extension would enable to see the differences in the strength of the adaptation as well as how is the recovery affected by a longer time period.

2. A pathway-specific adaptation?

Another point which offers experimental perspective is to test whether the adapted neurons are specific of the vestibulo-ocular pathway, or if other vestibular-dependent pathway are also affected? For instance, the vestibular system is crucial for postural control through the vestibulo-spinal pathway. Are the descending outputs from the vestibular neurons modified following VOR long term adaptation? If that is the case, is this compensated by a change of the ascending proprioceptive inputs to the vestibular neurons? As seen, many intriguing questions arise from the present VVM protocol which all would deserve specific experimental testing.

3. Mechanisms of VOR learning

At this point, the hypothesis of a modification of the affinity of the receptors is the only one which has not been specifically tested. We could do so by using antagonists for the main contributors of the excitatory glutamatergic responses in the MVN: NMDA and AMPA receptors. Following the previously described procedure (see Materials and Methods, 3.2. Whole-cell patch clamp recording protocol), eEPSCs would be recorded first without and then with antagonists (for example, for NMDA: D-APV and for AMPA: NBQX) and both responses would be compared. Using the antagonists will make it

possible to isolate the relative contribution of the NMDA and AMPA receptors, and to identify putative changes in the dynamic of the receptors.

4. A specific role for type A interneurons

As we found a change in the intrinsic properties of only type A neurons after VOR adaptation, we can wonder whether the observed synaptic plasticity only appears on this subpopulation of MVN neurons. Our results so far indicate that this is probably not the case, as the decrease in EPSC was observed on an average population constituted of a majority of type B neurons. So, if plasticity is not restricted to this population, what makes the type A neurons intrinsic properties more likely to be adapted?

To answer this question, we could record from only type A neurons, which are thought to be GABAergic, and study the effect of VOR adaptation. To allow recordings of only GABAergic neurons, it would be possible to use transgenic lines expressing fluorescence in this kind of neurons. In this work, I began to use three different transgenic lines, which allowed seeing the heterogeneous expression of the different GABAergic neurons in the MVN.

The distinction between type A and type B could also be done using the genetically-engineered mice strains GAD67, in which the mouse expresses fluorescent GABAergic neurons (type A), as well as the YFP strain, in which the mouse has fluorescent glutamatergic/glycinergic neurons (type B). Our lab already has the GAD-67 mouse strains and will soon receive the YFP mouse line. Future experiments will therefore be possible using this genetic approach.

Furthermore, using Sst-Cre and Pvalb-cre expressing tdTomato fluorescent protein, we can narrow down the possible existence of subtypes of type A neurons. Overall, it will enable to study how the VOR adaptation affects both subpopulations and to sort out MVN populations according to their neurotransmitter content.

Conclusions

In conclusion, the presented study provides evidence in favor of the plasticity in the brainstem. Concretely, that long-term VOR adaptation is consolidated within the vestibular nuclei at the synapse between the first and second-order vestibular neurons.

VOR memory is consolidated through a transfer from the cerebellum to the vestibular nuclei. This transfer mechanism for “system consolidation” is postulated to relieve the cerebellar cortex and make it capable of learning new motor skills (Nagao et al., 2013, Clopath et al., 2014). Comparable mechanisms have also been reported in models of non-motor memories, for instance declarative memory transferred from the hippocampus to the cerebral cortex (Frankland and Bontempi, 2005, Takashima et al., 2006, Durrant and Lewis, 2009), as well as for associative memories transferred from the antennal lobes to the mushroom bodies in invertebrates (Carcaud et al., 2015).

The perspective that not all neurons react equally regarding pathological situations motivates future investigation in this direction. Understanding the similarities and differences will help to understand the plastic mechanisms that guarantee vestibular homeostasis and provide options for future treatments and rehabilitations following vestibular deficits.

Bibliography

Adelman, G. & Smith, B. H. 1999. *Encyclopedia of neuroscience,* Amsterdam ; New York, Elsevier.

Akbarian, S., Berndl, K., Grusser, O. J., Guldin, W., Pause, M. & Schreiter, U. 1988. Responses of single neurons in the parietoinsular vestibular cortex of primates. *Ann N Y Acad Sci,* 545**,** 187-202.

Albus JS (1971) A theory of cerebellar function. Math Biosciences 10:25-61

Bagnall, M. W., Stevens, R. J. & Du Lac, S. 2007. Transgenic mouse lines subdivide medial vestibular nucleus neurons into discrete, neurochemically distinct populations. *J Neurosci,* 27**,** 2318-30.

Barrett, K. E. & Ganong, W. F. 2010. *Ganong's review of medical physiology,* New York, McGraw-Hill Medical.

Beraneck, M. & Cullen, K. E. 2007. Activity of vestibular nuclei neurons during vestibular and optokinetic stimulation in the alert mouse. *J Neurophysiol,* 98**,** 1549-65.

Beraneck, M., Hachemaoui, M., Idoux, E., Ris, L., Uno, A., Godaux, E., Vidal, P. P., Moore, L. E. & Vibert, N. 2003. Long-term plasticity of ipsilesional medial vestibular nucleus neurons after unilateral labyrinthectomy. *J Neurophysiol,* 90**,** 184-203.

Beraneck, M. & Idoux, E. 2012. Reconsidering the role of neuronal intrinsic properties and neuromodulation in vestibular homeostasis. *Front Neurol,* 3**,** 25.

Beraneck, M., Idoux, E., Uno, A., Vidal, P. P., Moore, L. E. & Vibert, N. 2004. Unilateral labyrinthectomy modifies the membrane properties of contralesional vestibular neurons. *J Neurophysiol,* 92**,** 1668-84.

Beraneck, M. & Straka, H. 2011. Vestibular signal processing by separate sets of neuronal filters. *J Vestib Res,* 21**,** 5-19.

Bergquist, F., Ludwig, M. & Dutia, M. B. 2008. Role of the commissural inhibitory system in vestibular compensation in the rat. *J Physiol,* 586**,** 4441-52.

Blazquez, P. M., Hirata, Y. & Highstein, S. M. 2004. The vestibulo-ocular reflex as a model system for motor learning: what is the role of the cerebellum? *Cerebellum,* 3**,** 188-92.

Boyden, E. S., Katoh, A. & Raymond, J. L. 2004. Cerebellum-dependent learning: the role of multiple plasticity mechanisms. *Annu Rev Neurosci,* 27**,** 581-609.

Broussard, D. M. & Kassardjian, C. D. 2004. Learning in a simple motor system. *Learn Mem,* 11**,** 127-36.

Buttner, U. & Lang, W. 1979. The vestibulocortical pathway: neurophysiological and anatomical studies in the monkey. *Prog Brain Res,* 50**,** 581-8.

Carcaud, J., Giurfa, M. & Sandoz, J. C. 2015. Parallel Olfactory Processing in the Honey Bee Brain: Odor Learning and Generalization under Selective Lesion of a Projection Neuron Tract. *Front Integr Neurosci,* 9**,** 75.

Clopath, C., Badura, A., De Zeeuw, C. I. & Brunel, N. 2014. A cerebellar learning model of vestibulo-ocular reflex adaptation in wild-type and mutant mice. *J Neurosci,* 34**,** 7203-15.

Cullen, K. E. 2012. The vestibular system: multimodal integration and encoding of self-motion for motor control. *Trends Neurosci,* 35**,** 185-96.

Du Lac, S. 1996. Candidate cellular mechanisms of vestibulo-ocular reflex plasticity. *Ann N Y Acad Sci,* 781**,** 489-98.

Durrant, M. & Aristotle 1993. *Aristotle's De anima in focus,* London ; New York, Routledge.

Durrant, S. & Lewis, P. A. 2009. Memory consolidation: tracking transfer with functional connectivity. *Curr Biol,* 19**,** R860-2.

Dutia, M. B., Lotto, R. B. & Johnston, A. R. 1995. Post-natal development of tonic activity and membrane excitability in mouse medial vestibular nucleus neurones. *Acta Otolaryngol Suppl,* 520 Pt 1**,** 101-4.

Eugene, D., Deforges, S., Guimont, F., Idoux, E., Vidal, P. P., Moore, L. E. & Vibert, N. 2007. Developmental regulation of the membrane properties of central vestibular neurons by sensory vestibular information in the mouse. *J Physiol,* 583**,** 923-43.

Eugene, D., Idoux, E., Beraneck, M., Moore, L. E. & Vidal, P. P. 2011. Intrinsic membrane properties of central vestibular neurons in rodents. *Exp Brain Res,* 210**,** 423-36.

Faulstich, M., Van Alphen, A. M., Luo, C., Du Lac, S. & De Zeeuw, C. I. 2006. Oculomotor plasticity during vestibular compensation does not depend on cerebellar LTD. *J Neurophysiol,* 96**,** 1187-95.

Felten, D. L., Józefowicz, R. F. & Netter, F. H. 2003. *Netter's Atlas of human neuroscience,* Teterboro, N. J., Icon Learning Systems.

Fox, J. G. 2007. *The mouse in biomedical research,* Amsterdam ; Boston, MA, Elsevier/Academic Press.

Frankland, P. W. & Bontempi, B. 2005. The organization of recent and remote memories. *Nat Rev Neurosci,* 6**,** 119-30.

Goldberg, J. M. & Oxford University Press. 2012. The vestibular system a sixth sense. New York ; Oxford: Oxford University Press,.

Kandel, E. R. 2013. *Principles of neural science,* New York, McGraw-Hill Medical.

Khan, S. & Chang, R. 2013. Anatomy of the vestibular system: a review. *NeuroRehabilitation,* 32**,** 437-43.

Kodama, M., Hard, J. J. & Naish, K. A. 2012. Temporal variation in selection on body length and date of return in a wild population of coho salmon, Oncorhynchus kisutch. *BMC Evol Biol,* 12**,** 116.

Lisberger, S. G. 1994. Neural basis for motor learning in the vestibuloocular reflex of primates. III. Computational and behavioral analysis of the sites of learning. *J Neurophysiol,* 72**,** 974-98.

Lisberger, S. G. & Pavelko, T. A. 1988. Brain stem neurons in modified pathways for motor learning in the primate vestibulo-ocular reflex. *Science,* 242**,** 771-3.

Lisberger, S. G., Pavelko, T. A. & Broussard, D. M. 1994. Responses during eye movements of brain stem neurons that receive monosynaptic inhibition from the flocculus and ventral paraflocculus in monkeys. *J Neurophysiol,* 72**,** 909-27.

Marr D (1969) A theory of cerebellar cortex. J Physiol 202:437-470

Masuda, N. & Amari, S. 2008. A computational study of synaptic mechanisms of partial memory transfer in cerebellar vestibulo-ocular-reflex learning. *J Comput Neurosci,* 24**,** 137-56.

Mcelvain, L. E., Bagnall, M. W., Sakatos, A. & Du Lac, S. 2010. Bidirectional plasticity gated by hyperpolarization controls the gain of postsynaptic firing responses at central vestibular nerve synapses. *Neuron,* 68**,** 763-75.

Menzies, J. R., Porrill, J., Dutia, M. & Dean, P. 2010. Synaptic plasticity in medial vestibular nucleus neurons: comparison with computational requirements of VOR adaptation. *PLoS One,* 5.

Mescher, A. L. & Junqueira, L. C. U. 2013. Junqueira's basic histology text and atlas. *McGraw-Hill's AccessMedicine.* 13th ed. New York, N.Y.: McGraw Hill Medical,.

Miles, F. A. & Lisberger, S. G. 1981. Plasticity in the vestibulo-ocular reflex: a new hypothesis. *Annu Rev Neurosci,* 4**,** 273-99.

Mitchell, D. E., Della Santina, C. C. & Cullen, K. E. 2016. Plasticity within non-cerebellar pathways rapidly shapes motor performance in vivo. *Nat Commun,* 7**,** 11238.

Murphy, G. J. & Du Lac, S. 2001. Postnatal development of spike generation in rat medial vestibular nucleus neurons. *J Neurophysiol,* 85**,** 1899-906.

Nagao, S., Honda, T. & Yamazaki, T. 2013. Transfer of memory trace of cerebellum-dependent motor learning in human prism adaptation: a model study. *Neural Netw,* 47**,** 72-80.

Porrill, J. & Dean, P. 2007. Cerebellar motor learning: when is cortical plasticity not enough? *PLoS Comput Biol,* 3**,** 1935-50.

Precht, W. & Shimazu, H. 1965. Functional connections of tonic and kinetic vestibular neurons with primary vestibular afferents. *J Neurophysiol,* 28**,** 1014-28.

Puyal, J., Grassi, S., Dieni, C., Frondaroli, A., Dememes, D., Raymond, J. & Pettorossi, V. E. 2003. Developmental shift from long-term depression to long-term potentiation in the rat medial vestibular nuclei: role of group I metabotropic glutamate receptors. *J Physiol,* 553**,** 427-43.

Ramachandran, R. & Lisberger, S. G. 2008. Neural substrate of modified and unmodified pathways for learning in monkey vestibuloocular reflex. *J Neurophysiol,* 100**,** 1868-78.

Ris, L., Hachemaoui, M., Vibert, N., Godaux, E., Vidal, P. P. & Moore, L. E. 2001. Resonance of spike discharge modulation in neurons of the guinea pig medial vestibular nucleus. *J Neurophysiol,* 86**,** 703-16.

Rossert, C. & Straka, H. 2011. Interactions between intrinsic membrane and emerging network properties determine signal processing in central vestibular neurons. *Exp Brain Res,* 210**,** 437-49.

Roy, J. E. & Cullen, K. E. 2001. Selective processing of vestibular reafference during self-generated head motion. *J Neurosci,* 21**,** 2131-42.

Sans, N. A., Montcouquiol, M. E. & Raymond, J. 2000. Postnatal developmental changes in AMPA and NMDA receptors in the rat vestibular nuclei. *Brain Res Dev Brain Res,* 123**,** 41-52.

Scarduzio, M., Panichi, R., Pettorossi, V. E. & Grassi, S. 2012. The repetition timing of high frequency afferent stimulation drives the bidirectional plasticity at central synapses in the rat medial vestibular nuclei. *Neuroscience,* 223**,** 1-11.

Scudder, C. A. & Fuchs, A. F. 1992. Physiological and behavioral identification of vestibular nucleus neurons mediating the horizontal vestibuloocular reflex in trained rhesus monkeys. *J Neurophysiol,* 68**,** 244-64.

Serafin, M., De Waele, C., Khateb, A., Vidal, P. P. & Muhlethaler, M. 1991. Medial vestibular nucleus in the guinea-pig. II. Ionic basis of the intrinsic membrane properties in brainstem slices. *Exp Brain Res,* 84**,** 426-33.

Shimazu, H. & Precht, W. 1965. Tonic and kinetic responses of cat's vestibular neurons to horizontal angular acceleration. *J Neurophysiol,* 28**,** 991-1013.

Shin, M., Moghadam, S. H., Sekirnjak, C., Bagnall, M. W., Kolkman, K. E., Jacobs, R., Faulstich, M. & Du Lac, S. 2011. Multiple types of cerebellar target neurons and their circuitry in the vestibulo-ocular reflex. *J Neurosci,* 31**,** 10776-86.

Squire, L. R. 2003. *Fundamental neuroscience,* Amsterdam ; San Diego, Calif. ; London, Academic Press.

Stahl, J. S. 2004. Eye movements of the murine P/Q calcium channel mutant rocker, and the impact of aging. *J Neurophysiol,* 91**,** 2066-78.

Straka, H., Vibert, N., Vidal, P. P., Moore, L. E. & Dutia, M. B. 2005. Intrinsic membrane properties of vertebrate vestibular neurons: function, development and plasticity. *Prog Neurobiol,* 76**,** 349-92.

Sun, Y., Waller, H. J., Godfrey, D. A. & Rubin, A. M. 2002. Spontaneous activity in rat vestibular nuclei in brain slices and effects of acetylcholine agonists and antagonists. *Brain Res,* 934**,** 58-68.

Takashima, A., Petersson, K. M., Rutters, F., Tendolkar, I., Jensen, O., Zwarts, M. J., Mcnaughton, B. L. & Fernandez, G. 2006. Declarative memory consolidation in humans: a prospective functional magnetic resonance imaging study. *Proc Natl Acad Sci U S A,* 103**,** 756-61.

Takazawa, T., Saito, Y., Tsuzuki, K. & Ozawa, S. 2004. Membrane and firing properties of glutamatergic and GABAergic neurons in the rat medial vestibular nucleus. *J Neurophysiol,* 92**,** 3106-20.

Wiest, G. 2015. The origins of vestibular science. *Ann N Y Acad Sci,* 1343**,** 1-9.

Yamazaki, T., Nagao, S., Lennon, W. & Tanaka, S. 2015. Modeling memory consolidation during posttraining periods in cerebellovestibular learning. *Proc Natl Acad Sci U S A,* 112**,** 3541-6.

Publications

Carcaud, J., França de Barros, F., Idoux, E., Eugène, D., Reveret, L., Moore, LE., Vidal, PP. & Beraneck, M. 2016. Brainstem plasticity following long-term adaptation of the vestibulo-1 ocular reflex. Manuscript under consideration.

Annexes

Annex 1. Example record sheet of the weight for one group. Each column has a parameter: “Mouse” - number on their microchip by which the mice are identificated; “Surgery” – day in which the surgery was done; “Adapted” – day of the conditioning with the adaptation device and “Day” – record of the weight (in grams) during protocol. Days marked with \ indicate days in which the weighting wasn’t done.

Mouse	**Surgery**	**Adapted**	**Day (weight in grams)**															
			0	1	2	3	4	5	6	7	8	9	10	11	12	13	14	15
4084402	08/10/2015	12/10/2015	17,3	17,4	18,1	18,7	19,4	\	\	21,1	21,2	21,5	21,9	22,1	\	\	22,5	23
4084168	08/10/2015	12/10/2015	18,1	18,9	19,2	19,5	20	\	\	19	18,9	18,6	18,6	18,8	\	\	20,5	21,2
4084391	08/10/2015	12/10/2015	19,2	19,7	19,9	20,4	20,5	\	\	19,9	19,3	18,9	19,3	20,1	\	\	21,6	22,4
4084417	08/10/2015	13/10/2015	20,6	20,2	20,2	20,4	\	\	19,8	19,7	20,2	20,3	20,8	\	\	22,5	22,2	23,3
4084179	08/10/2015	13/10/2015	18,8	19,6	19,6	19,7	\	\	21,7	22,1	22,4	22,6	22,6	\	\	23,5	23,4	23,9
4084117	08/10/2015	13/10/2015	19,8	19,7	19,8	19,7	\	\	18,9	17,9	18,2	18,4	19,1	\	\	20,5	20,8	21,5

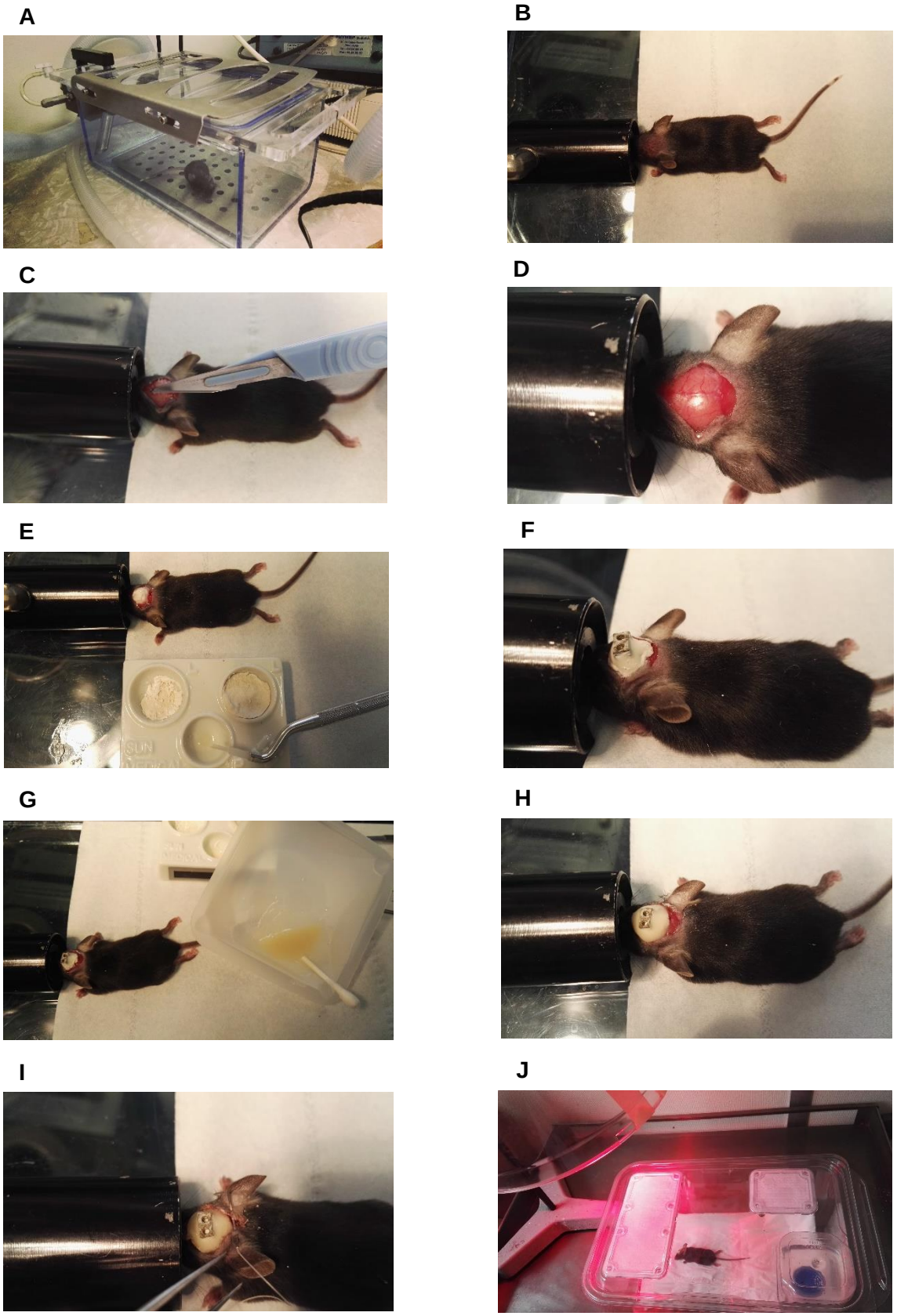

Annex 2. Surgical procedure steps for the headpost fixation. (A)Deep anesthesia with isoflurane; (B)preparation of the mouse to do (C, D) the first incision with the scalpel. (E, F, G, H) Cementing to the skull of the headpost, (I) suture and (J) recovery under the red-lights.

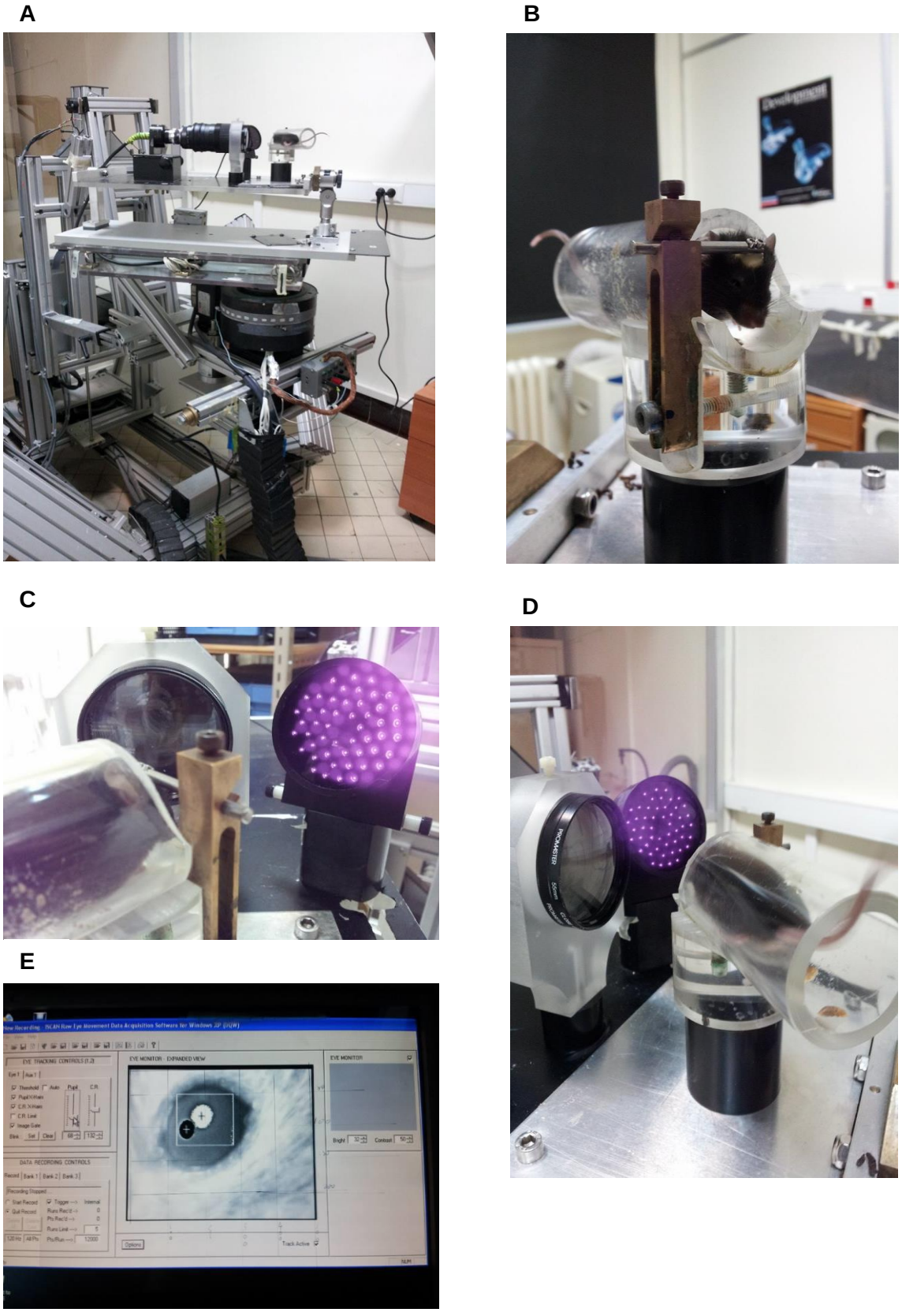

Annex 3. Video-oculography room. (A) Video-oculography device with motor and platforms. (B) Mouse in the Plexiglas tube used to immobilize. (C, D) Infrared light and camera that records the eye movements and in turn sends them to the computer (E) where the monitoring of the eye movements is done.